



This is a repository copy of *Model anionic block copolymer vesicles provide important design rules for efficient nanoparticle occlusion within calcite.*

White Rose Research Online URL for this paper:
<http://eprints.whiterose.ac.uk/143118/>

Version: Supplemental Material

Article:

Ning, Y. orcid.org/0000-0003-1808-3513, Han, L., Derry, M.J. orcid.org/0000-0001-5010-6725 et al. (2 more authors) (2019) Model anionic block copolymer vesicles provide important design rules for efficient nanoparticle occlusion within calcite. *Journal of the American Chemical Society*, 141 (6). pp. 2557-2567. ISSN 0002-7863

<https://doi.org/10.1021/jacs.8b12507>

This document is the Accepted Manuscript version of a Published Work that appeared in final form in *Journal of the American Chemical Society*, copyright © American Chemical Society after peer review and technical editing by the publisher. To access the final edited and published work see <https://doi.org/10.1021/jacs.8b12507>

Reuse

Items deposited in White Rose Research Online are protected by copyright, with all rights reserved unless indicated otherwise. They may be downloaded and/or printed for private study, or other acts as permitted by national copyright laws. The publisher or other rights holders may allow further reproduction and re-use of the full text version. This is indicated by the licence information on the White Rose Research Online record for the item.

Takedown

If you consider content in White Rose Research Online to be in breach of UK law, please notify us by emailing eprints@whiterose.ac.uk including the URL of the record and the reason for the withdrawal request.



eprints@whiterose.ac.uk
<https://eprints.whiterose.ac.uk/>

Model Anionic Block Copolymer Vesicles Provide Important Design Rules for Efficient Nanoparticle Occlusion within Calcite

Yin Ning,^{*,†} Lijuan Han,[†] Matthew J. Derry,[†] Fiona C. Meldrum,[‡] and Steven P. Armes^{*,†}

[†] Department of Chemistry, University of Sheffield, Brook Hill, Sheffield, South Yorkshire S3 7HF, U.K.

E-mail: Y.Ning@sheffield.ac.uk; s.p.arnes@sheffield.ac.uk.

[‡] School of Chemistry, University of Leeds, Woodhouse Lane, Leeds, LS2 9JT, U.K.

KEY WORDS: polymerization-induced self-assembly, block copolymer, vesicles, nanoparticle occlusion, calcite

1. Experimental Section

1.1. Materials

Glycerol monomethacrylate (GMA; 99.8%) was supplied by GEO Specialty Chemicals (Hythe, UK) and 2-(phosphonoxy)ethyl methacrylate (90%) was kindly donated by Solvay (France). Both of these two chemicals were used without further purification. 2-Hydroxypropyl methacrylate (HPMA), ethylene glycol dimethacrylate (EGDMA), fluorescein O-methacrylate (FMA; 97%), methacrylic acid, ammonium 2-sulfatoethyl methacrylate, potassium 3-sulfopropyl methacrylate, sodium 4-styrenesulfonate, 4,4'-azobis(4-cyanovaleric acid) (ACVA; 99%), 4-cyano-4-(phenylcarbonothioylthio)pentanoic acid (CPCP), ammonium carbonate and calcium chloride hexahydrate were all purchased from Sigma-Aldrich (UK) and used as received. Bindzil CC401 colloidal silica was kindly supplied as a 40 % w/w aqueous dispersion by AkzoNobel Pulp and Performance Chemicals AB (Sweden). Deionized water was obtained from an in-house Elgastat Option 3A water purification unit. All solvents were obtained from Sigma-Aldrich (UK).

1.2. Synthesis of poly(glycerol monomethacrylate) (G_{54}) macro-CTA

The synthesis of a G_{54} macro-CTA was conducted as follows. CPCP RAFT agent (1.12 g, 4 mmol), ACVA initiator (0.225 g, 0.80 mmol, CTA/ACVA molar ratio = 5.0) and anhydrous ethanol (33 g, 0.717 mol) were added to a round-bottomed flask containing a magnetic stirrer bar. When the CPCP and ACVA were fully dissolved to afford a pink solution, GMA monomer (32.0 g, 0.20 mol) was charged to target a mean degree of polymerization (DP) of 50. This reaction flask was immersed in an ice bath and purged with N_2 for 30 min, before being placed into an oil bath set at 70 °C. After 3 h, the polymerization was quenched by cooling the flask in ice, followed by exposure to air. The resulting polymer was purified by precipitation into a ten-fold excess of dichloromethane (twice). The moist precipitate was redissolved in water and the final polymer powder was obtained by lyophilization. 1H NMR analysis indicated a DP of 54 for this macro-CTA by comparing the integral from 0.5 ppm to 2.4 ppm assigned to the five methacrylic backbone protons with that of the signals

arising from the five aromatic protons on the RAFT CTA end-group. Taking into account the actual DP of 54 and the final monomer conversion of 90 %, this indicates a CTA efficiency of 83 % ($CTA\ efficiency = \frac{Target\ DP \times Monomer\ conversion}{True\ DP}$). DMF GPC analysis (vs. a series of poly(methyl methacrylate) calibration standards) indicated M_n and M_w/M_n values of $13,400\ g\ mol^{-1}$ and 1.17, respectively.

1.3. Synthesis of linear fluorescein-labeled poly(glycerol monomethacrylate)₅₄-poly(2-hydroxypropyl methacrylate)₃₅₀ (G₅₄-H₃₅₀) vesicles via RAFT aqueous dispersion polymerization

G₅₄ macro-CTA (0.1 g, 11.2 μ mol), ACVA initiator (0.63 mg, 2.24 μ mol, CTA/ACVA molar ratio = 5.0), FMA (3.0 mg, 7.49 μ mol), H₂O (5.992 g) and HPMA (0.565 g, 3.92 mmol) were successively weighed into a vial containing a magnetic stirrer bar. The vial was sealed and the reaction solution was degassed using N₂ gas for 30 min before being immersed in an oil bath set at 70 °C. The polymerization was quenched after 2.5 h and ¹H NMR analysis indicated a final monomer conversion of more than 99%.

1.4. Synthesis of cross-linked fluorescein-labeled poly(glycerol monomethacrylate)₅₄-poly(2-hydroxypropyl methacrylate)₃₅₀-poly(ethylene glycol dimethacrylate)₂₅ (G₅₄-H₃₅₀-E₂₅) vesicles via RAFT aqueous dispersion polymerization

G₅₄ macro-CTA (0.10 g, 11.2 μ mol), ACVA initiator (0.63 mg, 2.24 μ mol, CTA/ACVA molar ratio = 5.0), FMA (3.0 mg, 7.49 μ mol), H₂O (5.992 g) and HPMA (0.565 g, 3.92 mmol) were successively weighed into a glass vial containing a magnetic stir bar. This vial was sealed and the reaction solution was degassed using N₂ gas for 30 min. The vial was then immersed in an oil bath set at 70 °C. After 2.5 h, degassed EGDMA (55.5 mg, 0.28 mmol) was added to the reaction solution under N₂ and the polymerization was allowed to continue for a further 4 h. ¹H NMR analysis indicated a final monomer conversion of more than 99%.

1.5. In situ encapsulation of silica nanoparticles within cross-linked fluorescein-labeled poly(glycerol monomethacrylate)₅₄-poly(2-hydroxypropyl methacrylate)₃₅₀-poly(ethylene glycol dimethacrylate)₂₅ (G₅₄-H₃₅₀-E₂₅) vesicles via RAFT aqueous dispersion polymerization

G₅₄ macro-CTA (0.50 g, 0.056 mmol), ACVA initiator (3.14 mg, 11.2 μmol, CTA/ACVA molar ratio = 5.0), FMA (5.6 mg, 0.014 mmol), H₂O (11.235 g) and HPMA (2.826 g, 19.6 mmol) were successively weighed into a reaction flask containing a magnetic stir bar. Then Bindzil CC401 colloidal silica (18.73 g of a 40% w/w aqueous dispersion) was added to afford a silica concentration of 25% w/w. The flask was sealed and the reaction solution was degassed using N₂ gas for 30 min before being immersed in an oil bath set at 70 °C. After 2.5 h, degassed EGDMA (0.278 g, 1.4 mmol) was added to the reaction solution under N₂ and the polymerization was allowed to continue for a further 4 h. ¹H NMR analysis indicated a final monomer conversion of more than 99%. These silica-loaded G₅₄-H₃₅₀-E₂₅ ‘seed’ vesicles were then chain-extended using methacrylic acid (see below).

1.6. Chain extension of silica-loaded poly(glycerol monomethacrylate)₅₄-poly(2-hydroxypropyl methacrylate)₃₅₀-poly(ethylene glycol dimethacrylate)₂₅ (G₅₄-H₃₅₀-E₂₅) ‘seed’ vesicles with varying amounts of methacrylic acid

A typical protocol for the synthesis of silica-loaded poly(glycerol monomethacrylate)₅₄-poly(2-hydroxypropyl methacrylate)₃₅₀-poly(ethylene glycol dimethacrylate)₂₅-poly(methacrylic acid)₂₀₀ (G₅₄-H₃₅₀-E₂₅-MAA₂₀₀) is as follows. Precursor vesicles G₅₄-H₃₅₀-E₂₅ (3.357 g, 5.60 μmol) and ACVA (0.31 mg, 1.12 μmol) were added to a 30 mL glass vial containing a magnetic stir bar; then methacrylic acid (96.4 mg, 1.12 mmol), DMF (10 μL) and H₂O (5.165 g, 5 % w/w polymer solid concentration) were added. The reaction solution was stirred for 2 h and then purged with N₂ gas for 30 min before being immersed in an oil bath set at 70 °C for 24 h. ¹H NMR analysis indicated a final monomer conversion of more than 99%. The resulting silica-loaded G₅₄-H₃₅₀-E₂₅-MAA₂₀₀ vesicles were purified by six centrifugation-redispersion cycles (at 5,000 rpm for 30 min per cycle).

1.7. Chain extension of silica-loaded poly(glycerol monomethacrylate)₅₄-poly(2-hydroxypropyl methacrylate)₃₅₀-poly(ethylene glycol dimethacrylate)₂₅ (G₅₄-H₃₅₀-E₂₅) ‘seed’ vesicles with four different anionic monomers in turn when targeting a fixed DP of 300 in each case

A typical protocol for the synthesis of silica-loaded poly(glycerol monomethacrylate)₅₄-poly(2-hydroxypropyl methacrylate)₃₅₀-poly(ethylene glycol dimethacrylate)₂₅-poly(2-(phosphonooxy)ethyl methacrylate)₃₀₀ is as follows. Precursor vesicles G₅₄-H₃₅₀-E₂₅ (3.357 g, 5.60 μmol) and ACVA (0.31 mg, 1.12 μmol) were added to a 30 mL glass vial containing a magnetic stir bar; then 2-(phosphonooxy)ethyl methacrylate (353 mg, 1.68 mmol), DMF (10 μL, internal standard) and H₂O (10.93 g, 5.0 % w/w copolymer concentration) were added. The reaction solution was stirred for 2 h and then purged with N₂ gas for 30 min before being immersed in an oil bath set at 70 °C for 24 h. Then monomer conversion was measured to be more than 99% by ¹H NMR analysis. The resulting silica-loaded tetrablock copolymer vesicles were purified by six centrifugation-redispersion cycles (at 10,000 rpm for 30 min per cycle). Final monomer conversions were determined to be 97%, 97% and >99% for ammonium 2-sulfatoethyl methacrylate, potassium 3-sulfopropyl methacrylate and sodium 4-styrenesulfonate, respectively.

1.8. Precipitation of calcium carbonate crystals in the presence of silica-loaded G₅₄-H₃₅₀-E₂₅-MAA_x vesicles

An aqueous solution (10.0 mL) containing CaCl₂ (1.50 mM) and various vesicles (7.77 μM) was placed in a dessicator. CaCO₃ crystals were precipitated onto a glass slide placed at the base of this aqueous solution by exposure to ammonium carbonate vapor (2-3 g, placed at the bottom of the dessicator) for 24 h at 20 °C. Then the glass slide was removed from the solution and washed three times with deionized water, followed by three rinses with ethanol. Each occlusion experiment was repeated at least twice and consistent results were obtained in each case.

2. Characterization

2.1. ¹H NMR spectroscopy

All ¹H NMR spectra were recorded using a Bruker Avance 400 spectrometer operating at 400 MHz using D₂O, CD₃OD or d₆-DMSO as solvents.

2.2. Gel permeation chromatography (GPC)

The DMF GPC instrument set-up comprised two Polymer Laboratories PL gel 5 μm Mixed C columns and one PL polar gel 5 μm guard column connected in series to a Varian 390-LC multi-detector suite (only the refractive index detector was used) and a Varian 290-LC pump injection module operating at 60 °C. The GPC eluent was HPLC-grade DMF containing 10 mM LiBr and was filtered prior to use. The flow rate was 1.0 mL min⁻¹ and DMSO was used as a flow-rate marker. Calibration was conducted using a series of ten near-monodisperse poly(methyl methacrylate) standards ($M_n = 6.25 \times 10^2 - 6.18 \times 10^5 \text{ g mol}^{-1}$, $K = 2.094 \times 10^{-3}$, $\alpha = 0.642$). Chromatograms were analyzed using Varian Cirrus GPC software.

Aqueous GPC analysis was performed using an Agilent Technologies Infinity 1260 set-up equipped with two 8 μm PL Aquagel-OH 30 columns running at 30 °C equipped with two detectors (a UV detector set at 301 nm and a refractive index detector). The GPC eluent was an aqueous buffer comprising a mixture of 200 mM NaNO₃ and 10 mM NaH₂PO₄ at pH 9.1 and containing 30 vol% methanol at a flow rate of 1.0 mL min⁻¹. Calibration was achieved using a series of near-monodisperse poly(ethylene oxide) standards ranging from $6.20 \times 10^2 - 2.88 \times 10^5 \text{ g mol}^{-1}$.

2.3. Dynamic light scattering (DLS)

DLS measurements were conducted at 25 °C using a Malvern Zetasizer NanoZS instrument by detecting back-scattered light at an angle of 173°. Aqueous dispersions were diluted to 0.1% w/w using deionized water in the presence of 1.5 mM Ca²⁺ ions. The Stokes-Einstein equation was used to calculate z-average particle diameters. Aqueous electrophoresis measurements were conducted using disposable folded capillary cells supplied by Malvern (DTS1070) using the same Zetasizer NanoZS instrument in the presence of 1.5 mM CaCl₂.

2.4. Transmission electron microscopy (TEM)

TEM images were obtained using palladium-copper grids (Agar Scientific, UK). These grids were coated with a thin carbon film and then treated with a plasma glow discharge for approximately 30 seconds to create a hydrophilic surface prior to addition of the dilute aqueous dispersion (5 µL, 0.15 % w/v). Excess solvent was removed via blotting and the grid was stained with uranyl formate for 30 seconds. Excess stain was removed via blotting and the grid was carefully dried under vacuum. Imaging was performed using a FEI Tecnai G2 Spirit instrument operating at 80 kV.

2.5. Scanning electron microscopy (SEM)

Individual calcite crystals were fractured by placing a clean glass slide on top of the glass slide supporting the crystals, pressing down lightly and twisting one slide relative to the other. The resulting randomly-fractured calcite crystals were gold-coated (15 mA, 30 seconds) and then examined by scanning electron microscopy (FEI Inspect F). A relatively low accelerating voltage (5 kV) was applied in order to prevent sample charging. Focused ion beam (FIB) milling studies were performed using a FEI Quanta 200 3D instrument to prepare cross-sections through individual crystals. FIB milling was conducted using a gallium ion current (initially 7.0 nA, gradually reduced to 0.5 nA)

at an acceleration voltage of 30 kV. A final polish was conducted using a gallium ion current of 0.1 nA.

2.6. Other measurements

Fluorescence microscopy images were recorded using a Zeiss Axio Scope A1 microscope equipped with an AxioCam 1Cm1 monochrome camera. Images were captured and processed using ZEN lite 2012 software. Optical microscopy images were recorded using a Motic DMBA300 digital biological microscope equipped with a built-in camera and analyzed using Motic Images Plus 2.0 ML software. Raman spectra were recorded using a Renishaw 2000 Raman microscope equipped with a 785 nm diode laser. Thermogravimetric analyses (TGA) were conducted using a Perkin-Elmer Pyris 1 TGA instrument by heating dried calcite crystals from 30 °C to 900 °C in air at a heating rate of 10 °C per min. The samples were ground and dried at 110 °C for one week prior to TGA studies.

3. Extent of occlusion calculation based on TGA data

The block copolymer vesicles are completely pyrolyzed on heating to 500 °C and CaCO₃ is fully decomposed into CaO and CO₂ on heating to 800 °C (see **Figure S23**). Thus the extent of vesicle occlusion can be calculated from these TGA data. For example, if we assume that the relative mass contents % for the G₅₄-H₃₅₀-E₂₅-MAA₁₅₀ vesicles, SiO₂, CaO and CO₂ are x, y, m, and n, respectively, then the following four equations (S1-S4) can be obtained:

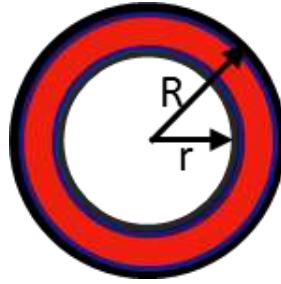
$$91.6 \% \times y + m = 52.3 \quad (\text{S1})$$

$$x + n = 100 - 52.3 \quad (\text{S2})$$

$$56 \times n = 44 \times m \quad (\text{S3})$$

$$91.6 \% \times y = 15.7\% \times (x + y) \quad (\text{S4})$$

Solving the above equations, $x = 7.76$, $y = 1.47$ and $m = 50.83$, and $n = 39.94$



The cartoon shown above indicates the outer radius (R) and inner radius (r) of the vesicles (with the stabilizer chains in the inner and outer leaflets shown in black). Thus the effective density of such vesicles, $\rho_{effective}$, can be calculated as follows.

$$\rho_{effective} = \frac{(R^3 - r^3) \times \rho_{vesicle}}{R^3}$$

The vesicle membrane thickness ($T = 36 \pm 5$ nm) can be estimated by TEM analysis and the overall mean vesicle diameter ($2R$) was obtained by DLS analysis. The solid-state density of the dried vesicles ($\rho_{vesicle}$) was determined by helium pycnometry at 20 °C (Micrometrics AccuPyc 1330 helium pycnometer). Given that the extent of vesicle occlusion within calcite by mass (x) can be determined by TGA, then the extent of vesicle occlusion by volume (x') can be calculated using the following equation:

$$x' = \frac{\frac{xR^3}{(R^3 - r^3)\rho_{vesicle}}}{\left[\frac{xR^3}{(R^3 - r^3)\rho_{vesicle}} + \frac{m+n}{\rho_{calcite}}\right]} \times 100 \%$$

Thus the extent of $G_{54}\text{-H}_{350}\text{-E}_{25}\text{-MAA}_{150}$ vesicle occlusion was calculated to be 41.3% (or approximately 41%) by volume.

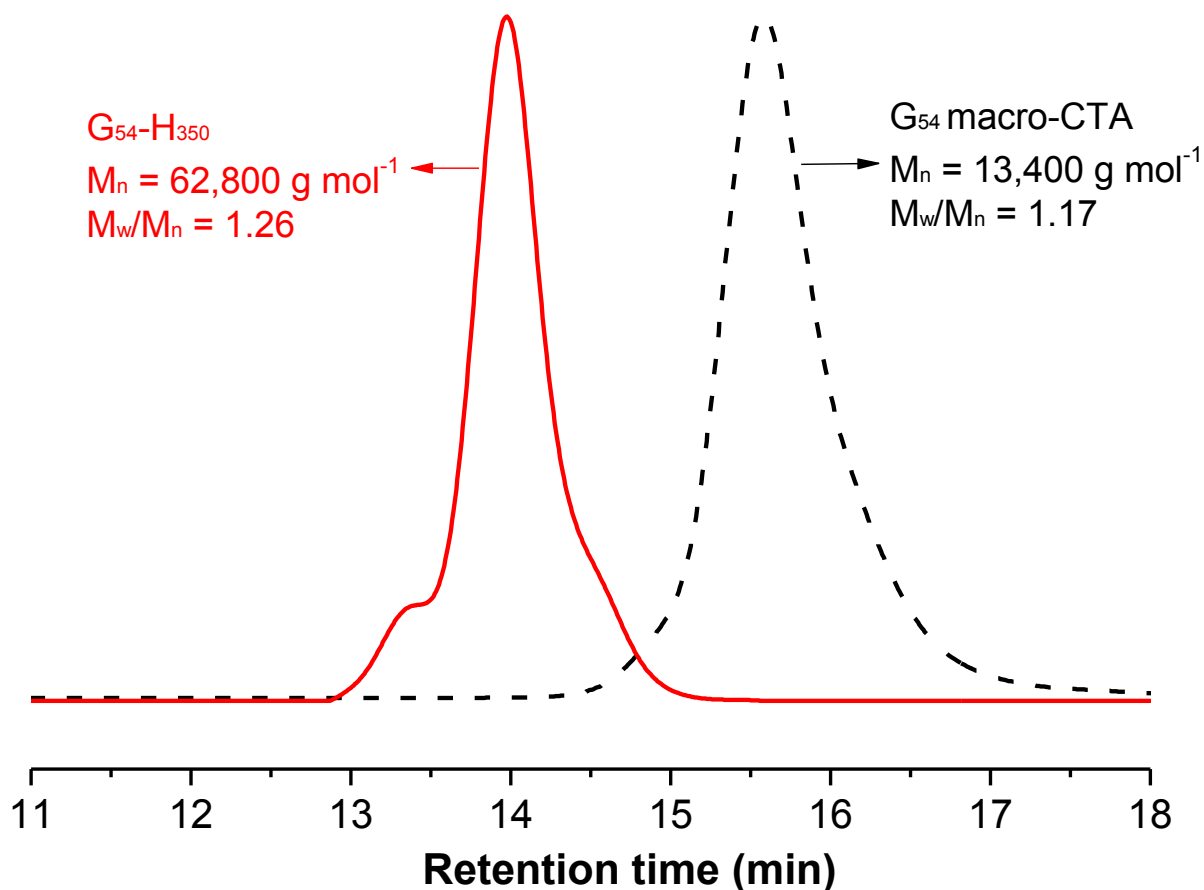


Figure S1. DMF GPC curves obtained for G_{54} macro-CTA and $G_{54}\text{-H}_{350}$ diblock copolymer (versus poly(methyl methacrylate) (PMMA) calibration standards). The shoulder observed for $G_{54}\text{-H}_{350}$ diblock copolymer was attributed to small amounts of a dimethacrylate impurity within the HPMA monomer, which leads to light branching of the PHPMA chains.¹⁻² This phenomenon has been commonly observed for this type of diblock copolymer.³⁻⁵

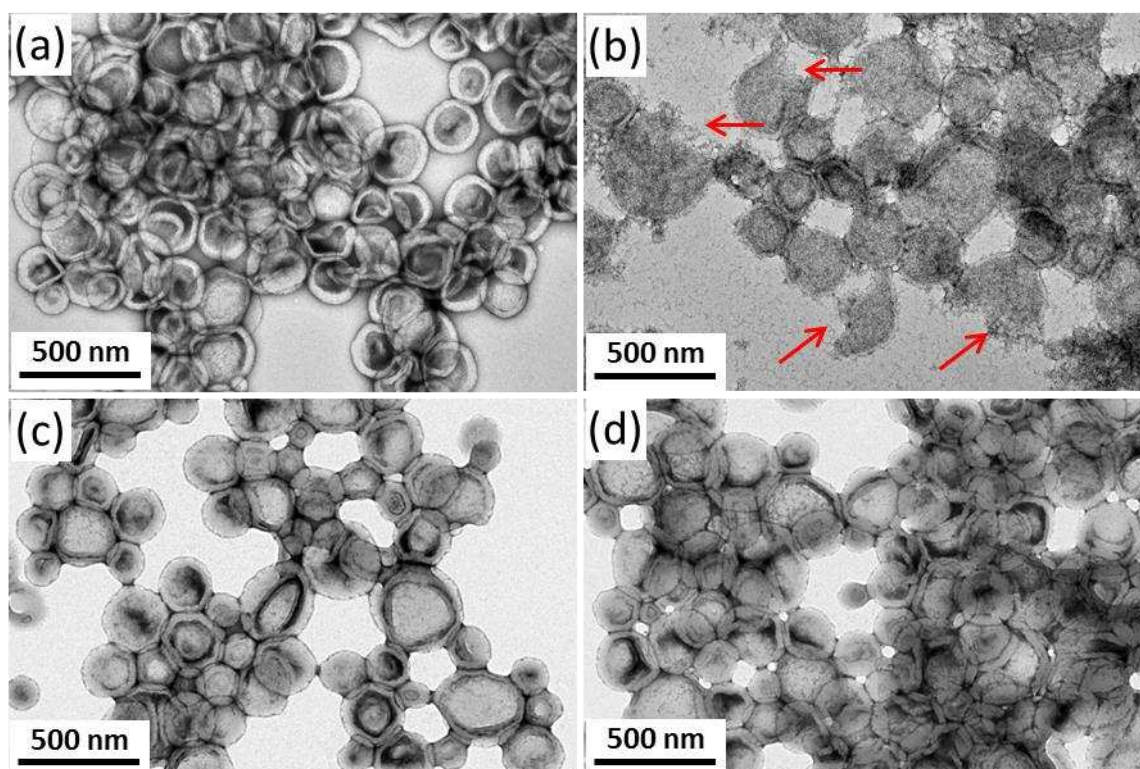


Figure S2. Transmission electron microscopy (TEM) images recorded for: (a) $G_{54}\text{-}H_{350}$; (b) $G_{54}\text{-}H_{350}\text{-}MAA_{150}$; (c) $G_{54}\text{-}H_{350}\text{-}E_{25}$; (d) $G_{54}\text{-}H_{350}\text{-}E_{25}\text{-}MAA_{150}$. The red arrows shown in (b) indicate that loss of the vesicular morphology occurs if linear precursor vesicles are chain-extended using methacrylic acid.

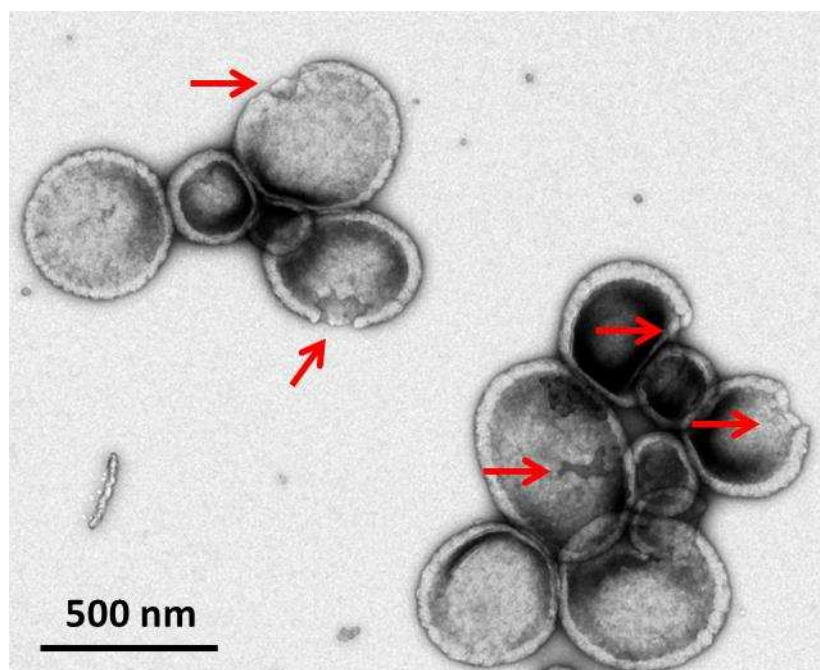


Figure S3. TEM images recorded for $G_{54}\text{-H}_{350}\text{-E}_{15}\text{-MAA}_{150}$ vesicles. The red arrows indicate disruption or cracking of the vesicle membrane. This is because 15 units of ethylene glycol dimethacrylate (denoted as E) cross-linker are not sufficient to covalently stabilize the vesicles. However, the original vesicular morphology was fully preserved when such vesicles were cross-linked with 25 E units, as shown in **Figure S2**.

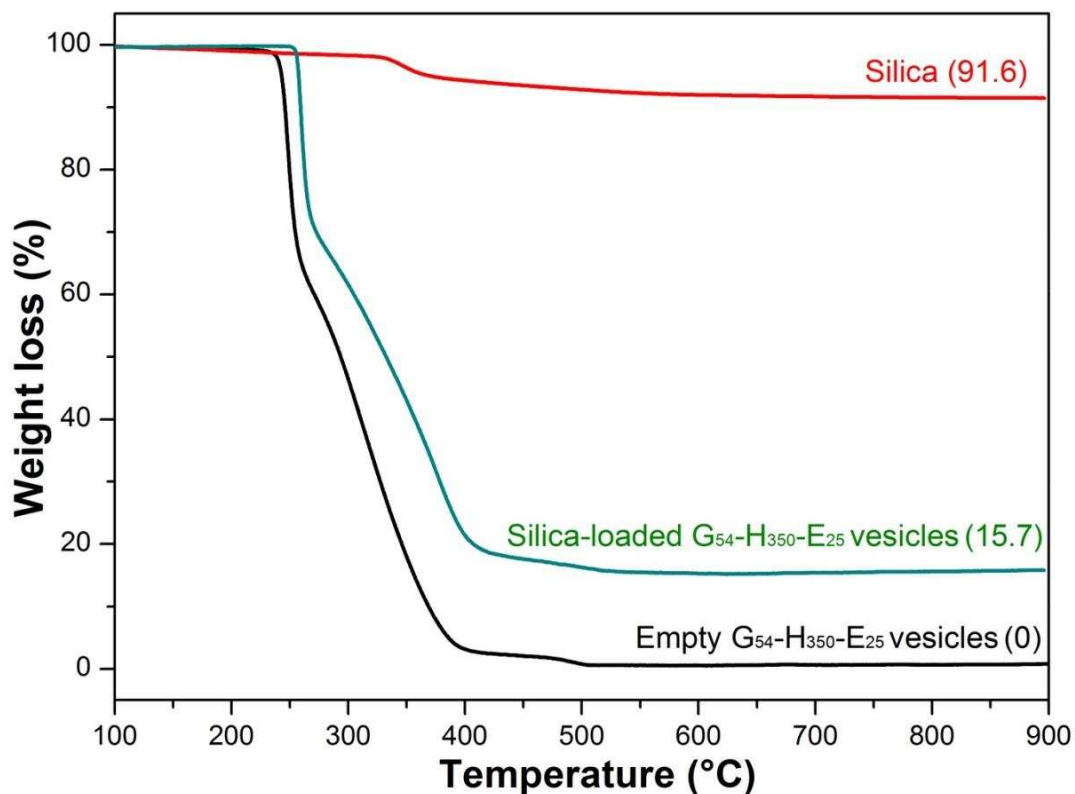


Figure S4. Thermogravimetric analysis (TGA) recorded for silica alone, silica-loaded crosslinked $G_{54}\text{-H}_{350}\text{-E}_{25}$ vesicles and empty crosslinked $G_{54}\text{-H}_{350}\text{-E}_{25}$ vesicles. These data indicate a mean silica loading of 17.1% by mass.

Calculation of the silica content of the vesicles in mass % from the TGA data shown in **Figure S4** requires correction. The dried silica sol exhibited some mass loss (8.4 %) on heating owing to partial surface dehydration. Thus the total ash in mass %, A , obtained after pyrolysis of the silica-loaded crosslinked $G_{54}\text{-H}_{350}\text{-E}_{25}$ vesicles, is given by the following equation:

$$A = \frac{\text{Silica} \times 91.6\%}{\text{Silica} + \text{Vesicle}}$$

Inspecting the TGA curve obtained for silica-loaded vesicles shown in **Figure S4**, $A = 15.7\%$. Hence the silica content within these vesicles expressed in mass % can be calculated as follows:

$$\text{Silica content of the vesicles in mass\%} = \frac{\text{Silica}}{\text{Silica} + \text{Vesicle}} = 17.1\%$$

Thus, the silica encapsulation efficiency is 9.9 %.

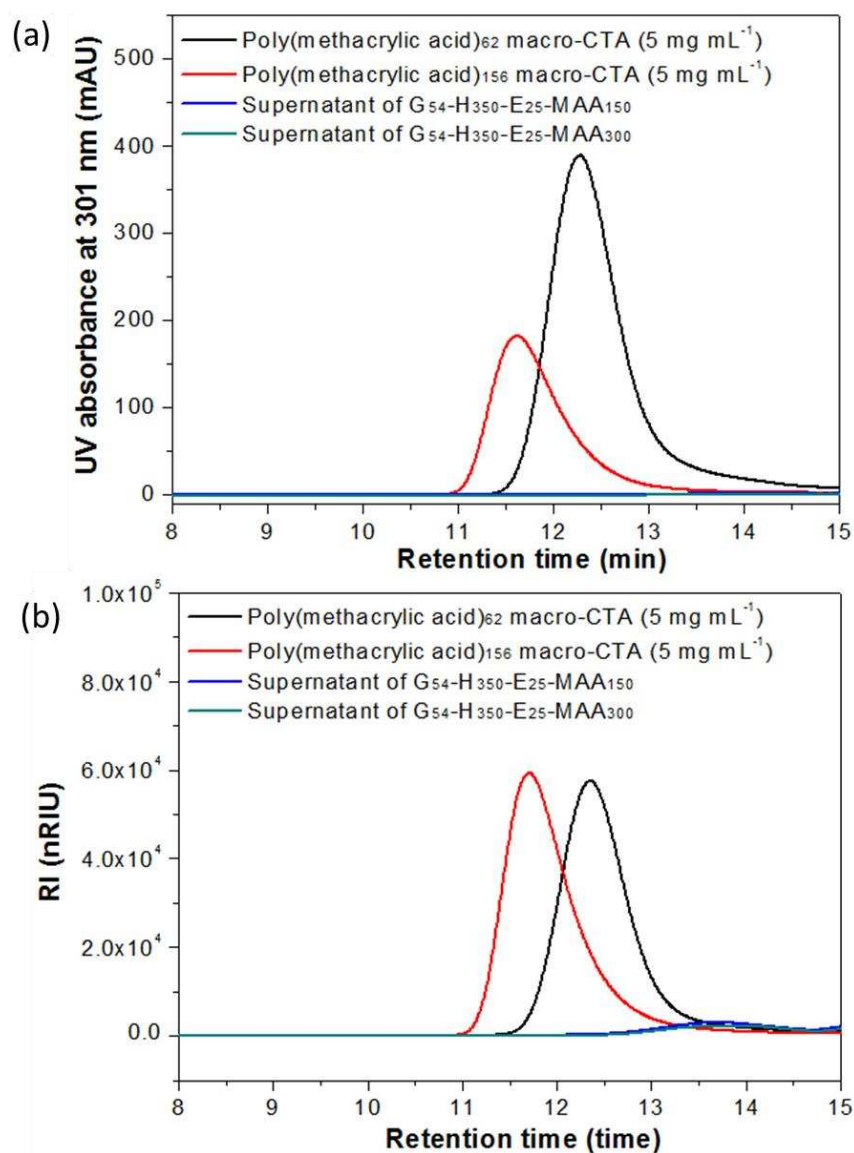


Figure S5. Aqueous GPC data recorded for poly(methacrylic acid)₆₂ macro-CTA, poly(methacrylic acid)₁₅₆ macro-CTA, and the two aqueous supernatants obtained after centrifugation of the G₅₄-H₃₅₀-E₂₅-MAA₁₅₀ vesicles and G₅₄-H₃₅₀-E₂₅-MAA₃₀₀ vesicles, respectively. N.B. The two poly(methacrylic acid) macro-CTAs were synthesized using CPCP as a RAFT agent, which has a UV absorbance at ~301 nm. **Figure S5a** shows no absorbance is observed at this wavelength for either aqueous supernatant, as expected. **Figure S5b** indicates that only very weak refractive index signals for relatively low molecular weight species were detected in the aqueous supernatants corresponding to the G₅₄-H₃₅₀-E₂₅-MAA₁₅₀ vesicles and G₅₄-H₃₅₀-E₂₅-MAA₃₀₀ vesicles, thus confirming minimal free poly(methacrylic acid) in the continuous phase.

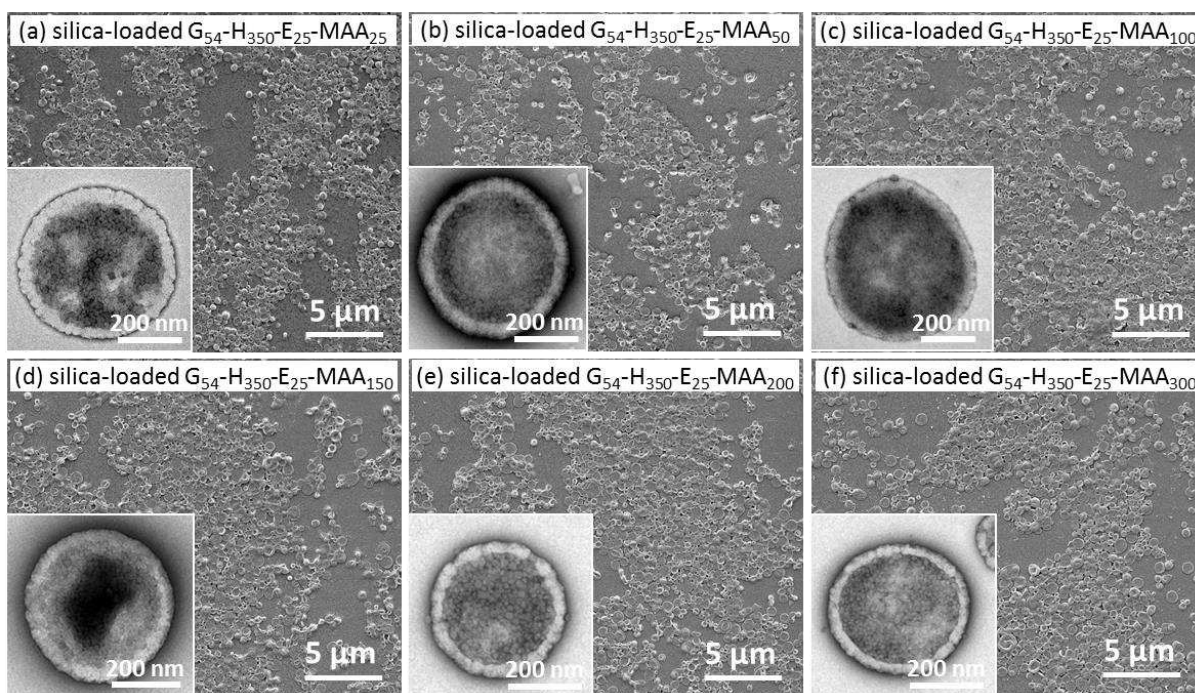


Figure S6. SEM images recorded for silica-loaded cross-linked $G_{54}\text{-H}_{350}\text{-E}_{25}\text{-MAA}_x$ vesicles (prepared using cross-linked $G_{54}\text{-H}_{350}\text{-E}_{25}$ precursor vesicles containing 17.1% silica by mass) prepared by targeting DPs of 25 to 300 for the poly(methacrylic acid) block. Clearly, there is no change in either the overall size or morphology of these $G_{54}\text{-H}_{350}\text{-E}_{25}\text{-MAA}_x$ vesicles, regardless of the poly(methacrylic acid) block DP. Insets show representative high magnification TEM images obtained for individual particles that confirm their vesicular morphology.

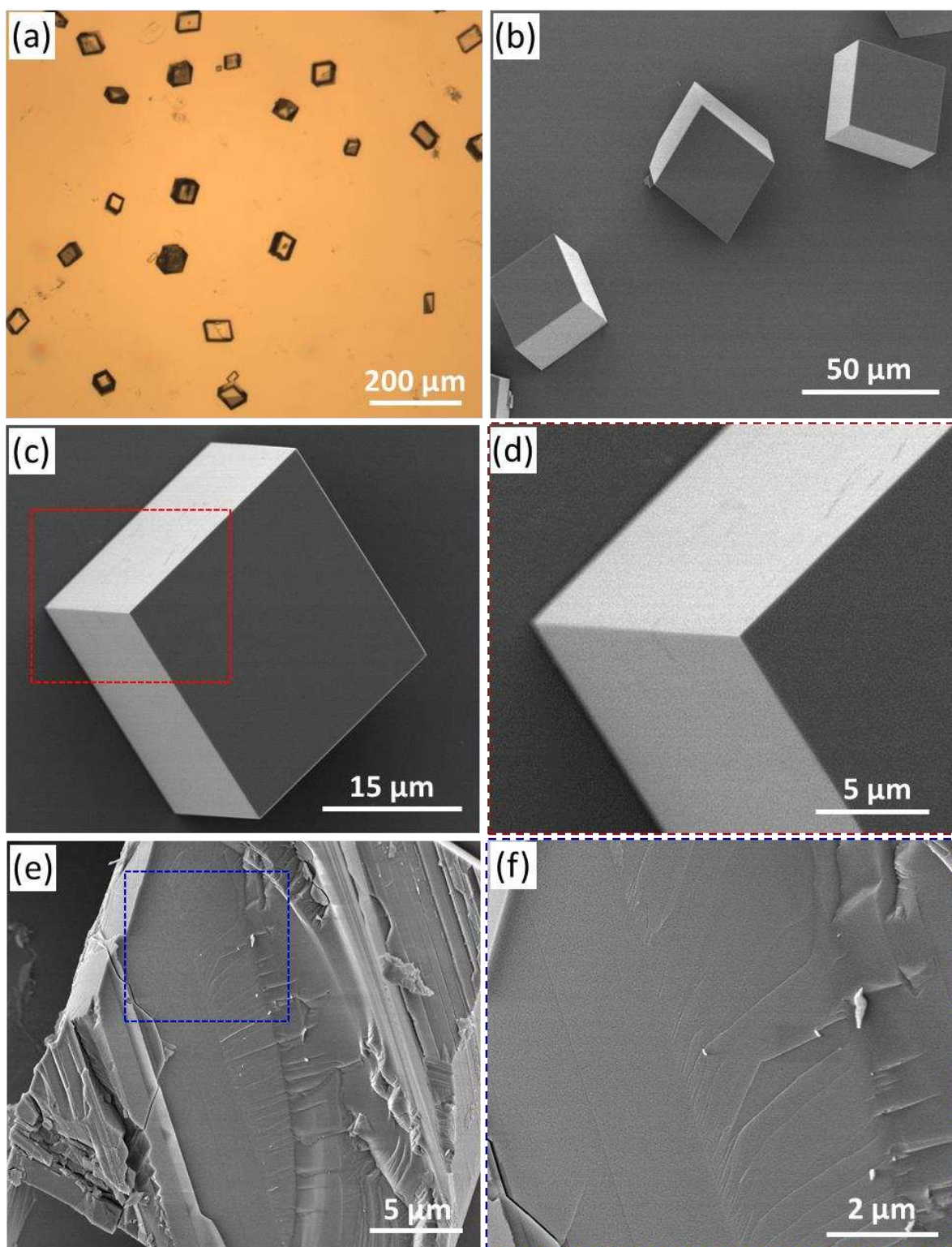


Figure S7. Calcite control crystals precipitated in the absence of any additive: (a) optical microscopy image; (b)~(d) SEM images, where (d) shows the area indicated in (c) at higher magnification; (e) SEM image showing the cross-section of a randomly-fractured crystal; (f) a high magnification SEM image showing the area indicated in (e).

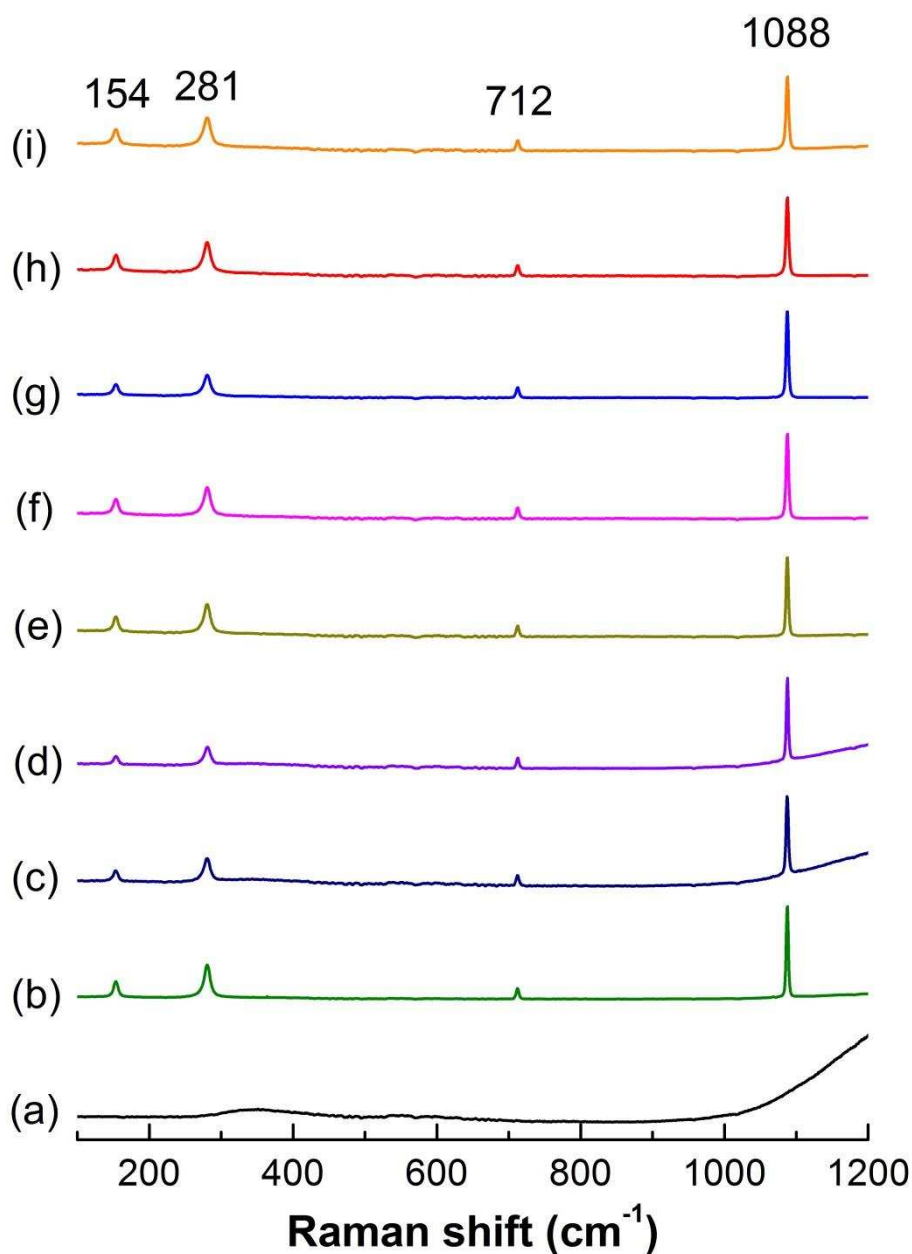


Figure S8. Raman spectra recorded for: (a) silica-loaded $G_{54}\text{-H}_{350}\text{-E}_{25}$ vesicles; (b) calcite control; (c)-(i) calcite crystals precipitated in the presence of a series of silica-loaded $G_{54}\text{-H}_{350}\text{-E}_{25}\text{-MAA}_x$ vesicles. More specifically, the vesicle compositions are: (c) silica-loaded $G_{54}\text{-H}_{350}\text{-E}_{25}$ vesicles, (d) silica-loaded $G_{54}\text{-H}_{350}\text{-E}_{25}\text{-MAA}_{25}$ vesicles, (e) silica-loaded $G_{54}\text{-H}_{350}\text{-E}_{25}\text{-MAA}_{50}$ vesicles, (f) silica-loaded $G_{54}\text{-H}_{350}\text{-E}_{25}\text{-MAA}_{100}$ vesicles, (g) silica-loaded $G_{54}\text{-H}_{350}\text{-E}_{25}\text{-MAA}_{150}$ vesicles, (h) silica-loaded $G_{54}\text{-H}_{350}\text{-E}_{25}\text{-MAA}_{200}$ vesicles and (i) silica-loaded $G_{54}\text{-H}_{350}\text{-E}_{25}\text{-MAA}_{300}$ vesicles. The peaks at 1088 cm^{-1} (ν_1), 712 cm^{-1} (ν_4), 281 cm^{-1} and 154 cm^{-1} (lattice modes) are characteristic of calcite.⁶⁻⁷

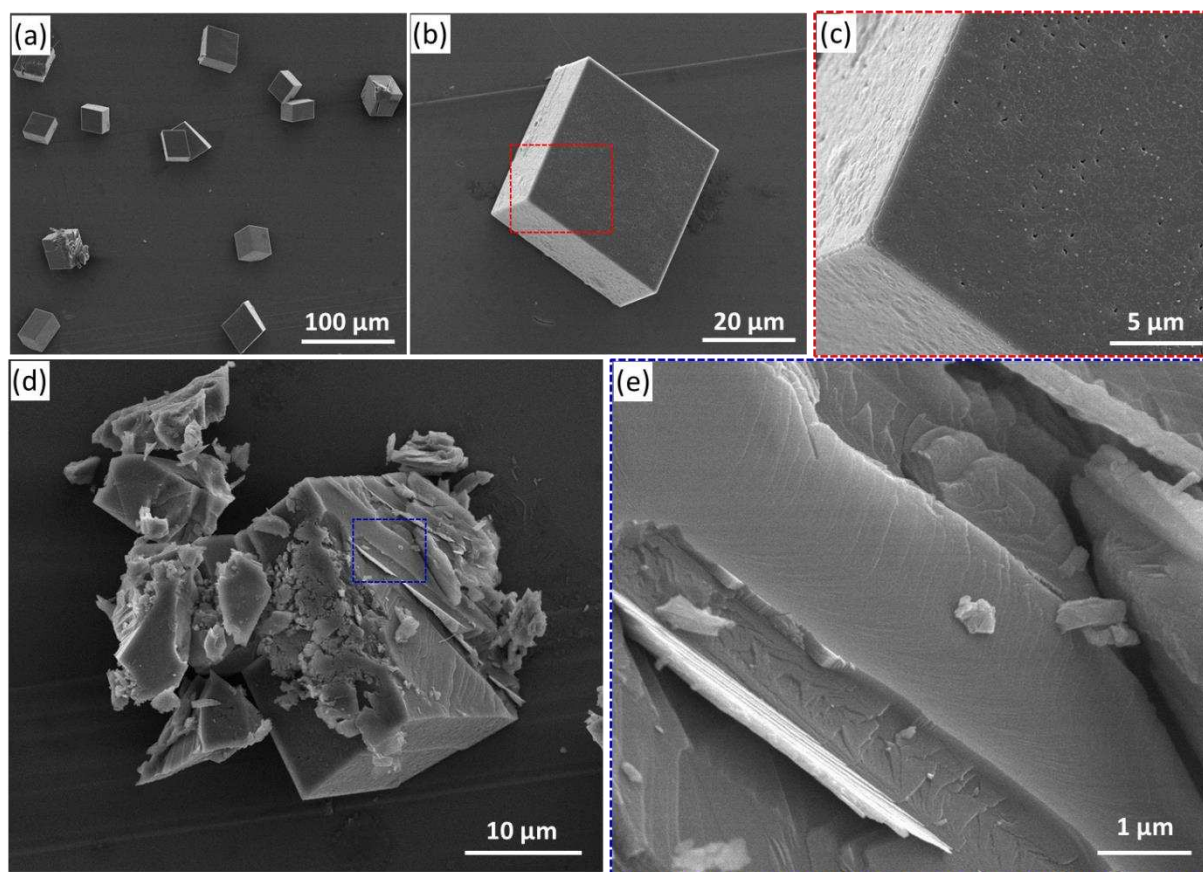


Figure S9. Calcite crystals precipitated in the presence of $7.77 \mu\text{M}$ silica-loaded $G_{54}\text{-H}_{350}\text{-E}_{25}$ vesicles. (a)~(c) SEM images, where (c) showing a magnified area as indicated in (b); (d) SEM image showing the cross-section of a randomly-fractured crystal; (e) a magnified SEM showing the area as indicated in (d).

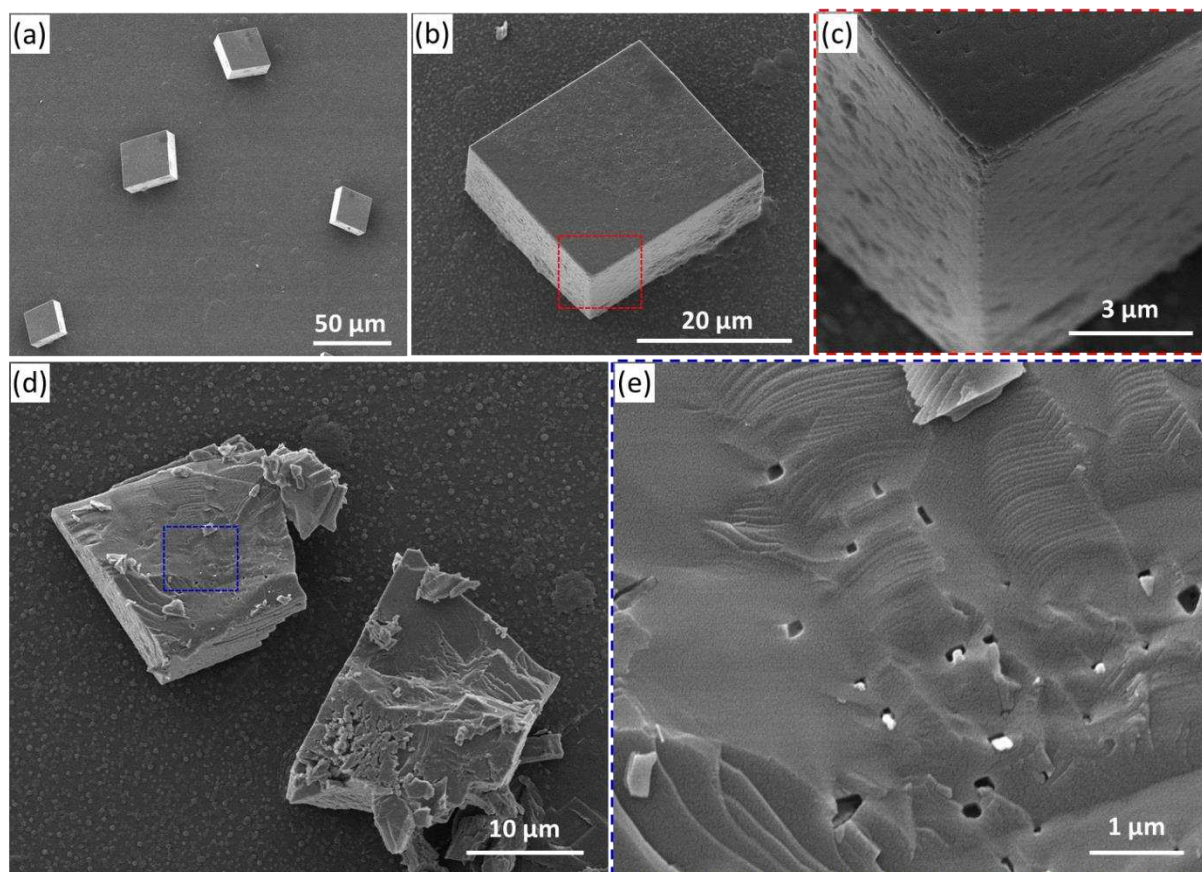


Figure S10. Calcite crystals precipitated in the presence of 7.77 μM silica-loaded G₅₄-H₃₅₀-E₂₅-MAA₂₅ vesicles. (a)~(c) SEM images, where (c) showing a magnified area as indicated in (b); (d) SEM image showing the cross-section of a randomly-fractured crystal; (e) a magnified SEM showing the area as indicated in (d).

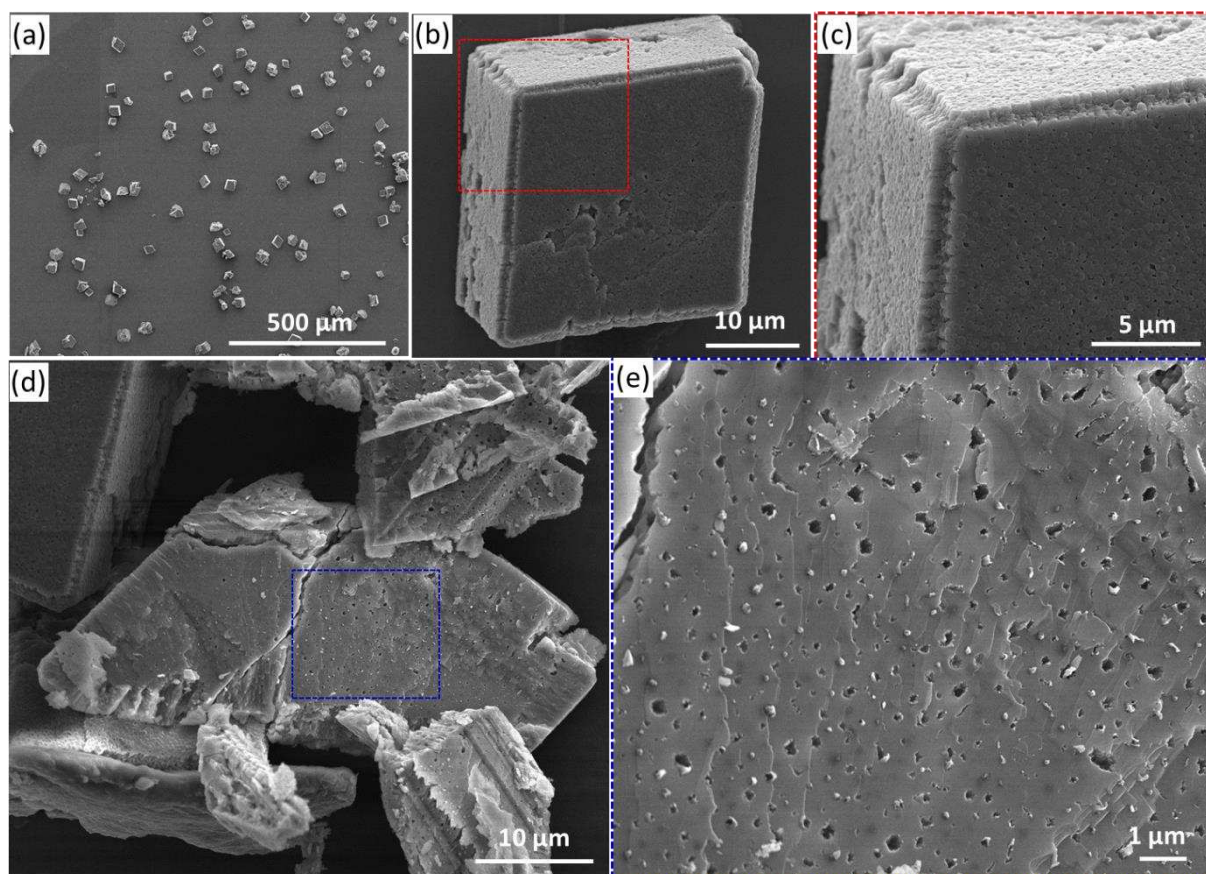


Figure S11. Calcite crystals precipitated in the presence of $7.77 \mu\text{M}$ silica-loaded $\text{G}_{54}\text{-H}_{350}\text{-E}_{25}\text{-MAA}_{50}$ vesicles. (a)~(c) SEM images, where (c) showing a magnified area as indicated in (b); (d) SEM image showing the cross-section of a randomly-fractured crystal; (e) a magnified SEM showing the area as indicated in (d).

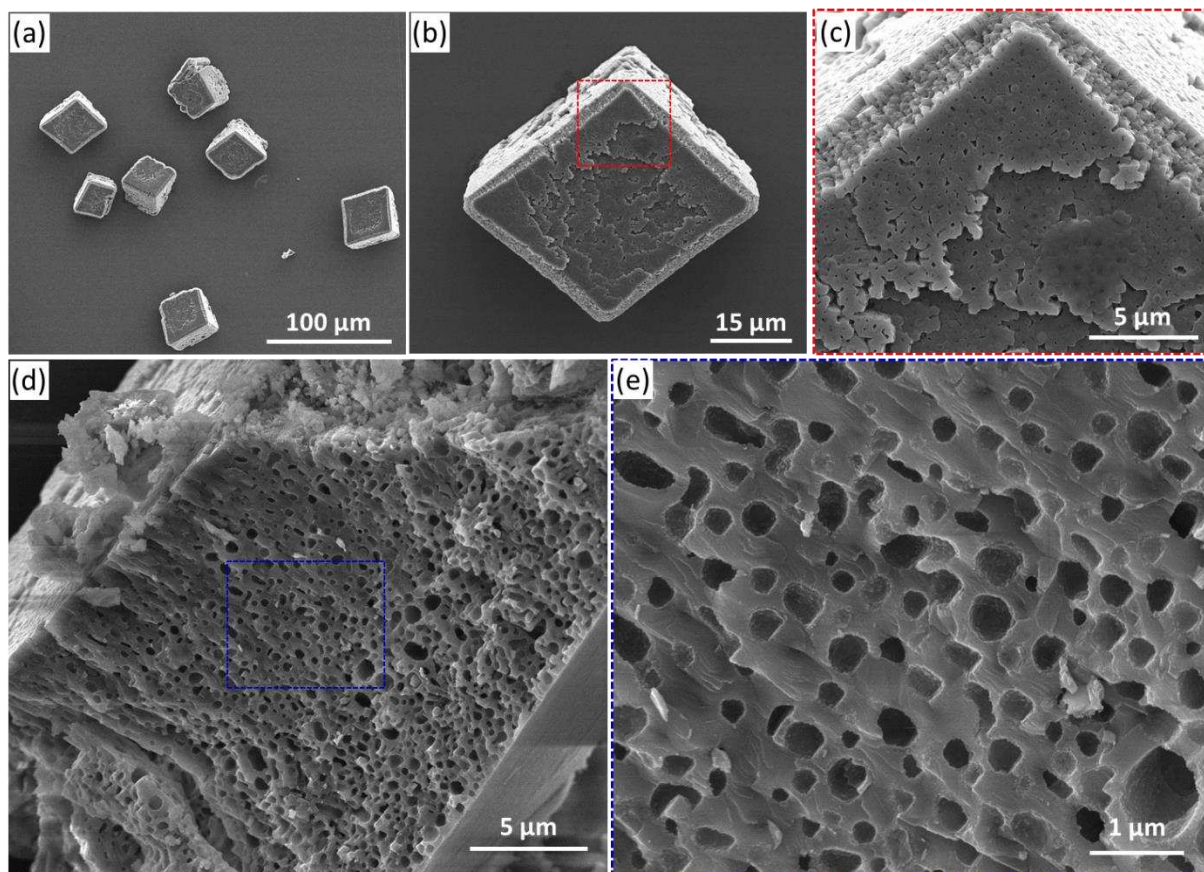


Figure S12. Calcite crystals precipitated in the presence of $7.77 \mu\text{M}$ silica-loaded $\text{G}_{54}\text{-H}_{350}\text{-E}_{25}\text{-MAA}_{100}$ vesicles. (a)~(c) SEM images, where (c) showing a magnified area as indicated in (b); (d) SEM image showing the cross-section of a randomly-fractured crystal; (e) a magnified SEM showing the area as indicated in (d).

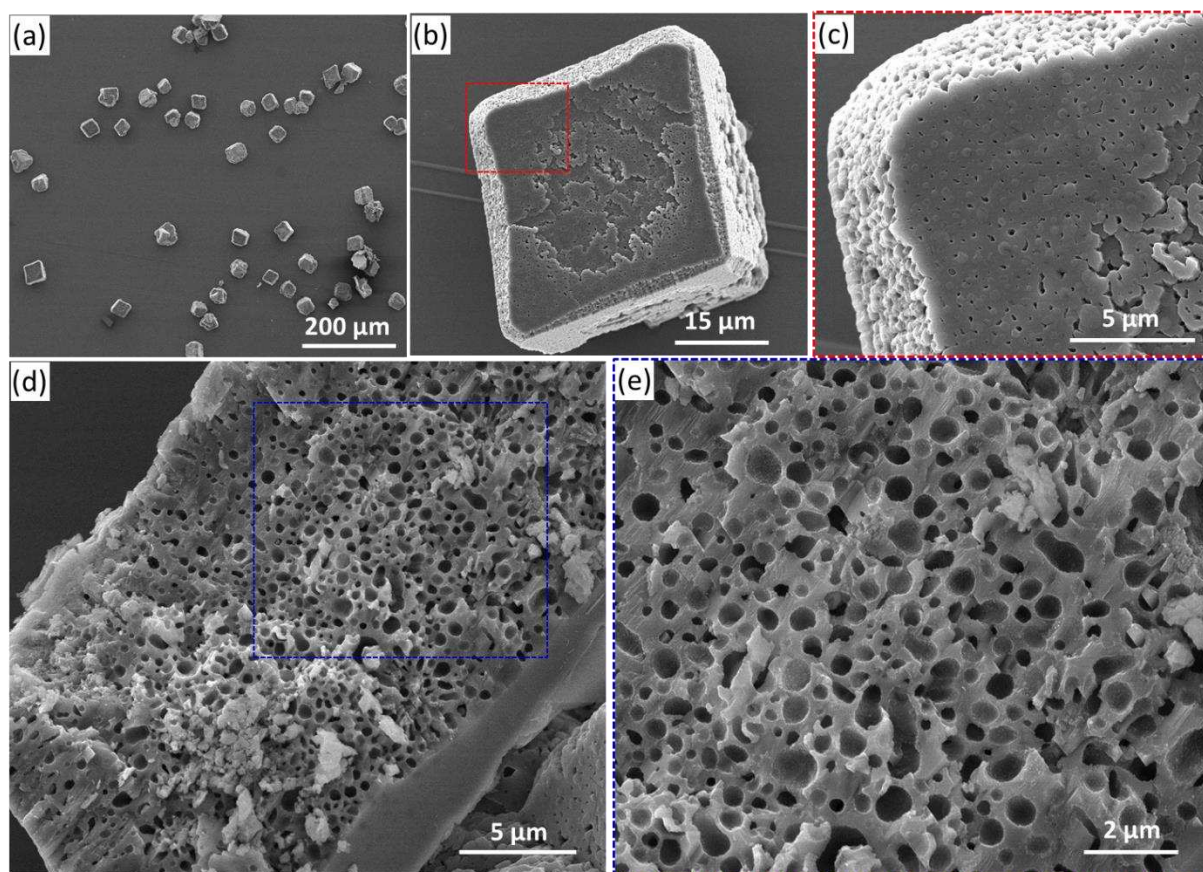


Figure S13. Calcite crystals precipitated in the presence of $7.77 \mu\text{M}$ silica-loaded $\text{G}_{54}\text{-H}_{350}\text{-E}_{25}\text{-MAA}_{150}$ vesicles. (a)~(c) SEM images, where (c) showing a magnified area as indicated in (b); (d) SEM image showing the cross-section of a randomly-fractured crystal; (e) a magnified SEM showing the area as indicated in (d).

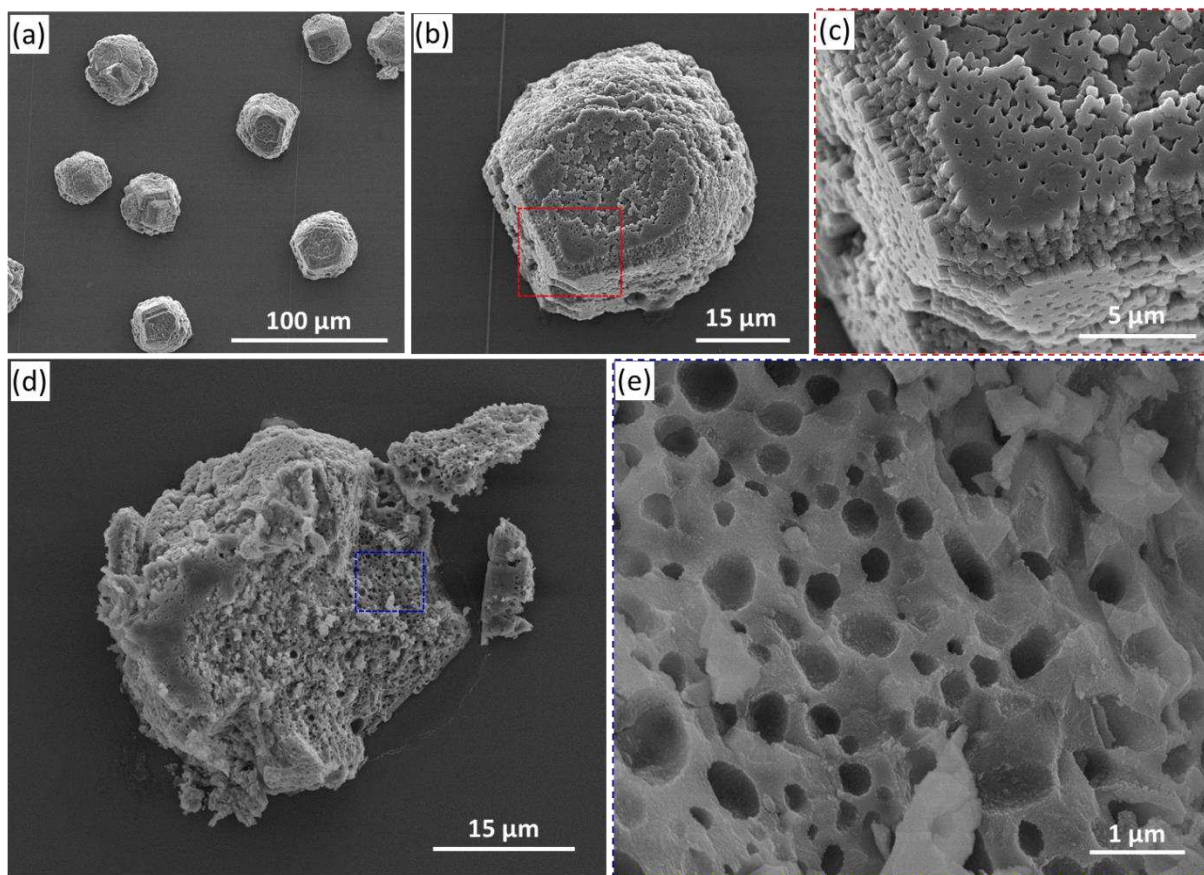


Figure S14. Calcite crystals precipitated in the presence of 7.77 μM silica-loaded G₅₄-H₃₅₀-E₂₅-MAA₂₀₀ vesicles. (a)~(c) SEM images, where (c) showing a magnified area as indicated in (b); (d) SEM image showing the cross-section of a randomly-fractured crystal; (e) a magnified SEM showing the area as indicated in (d).

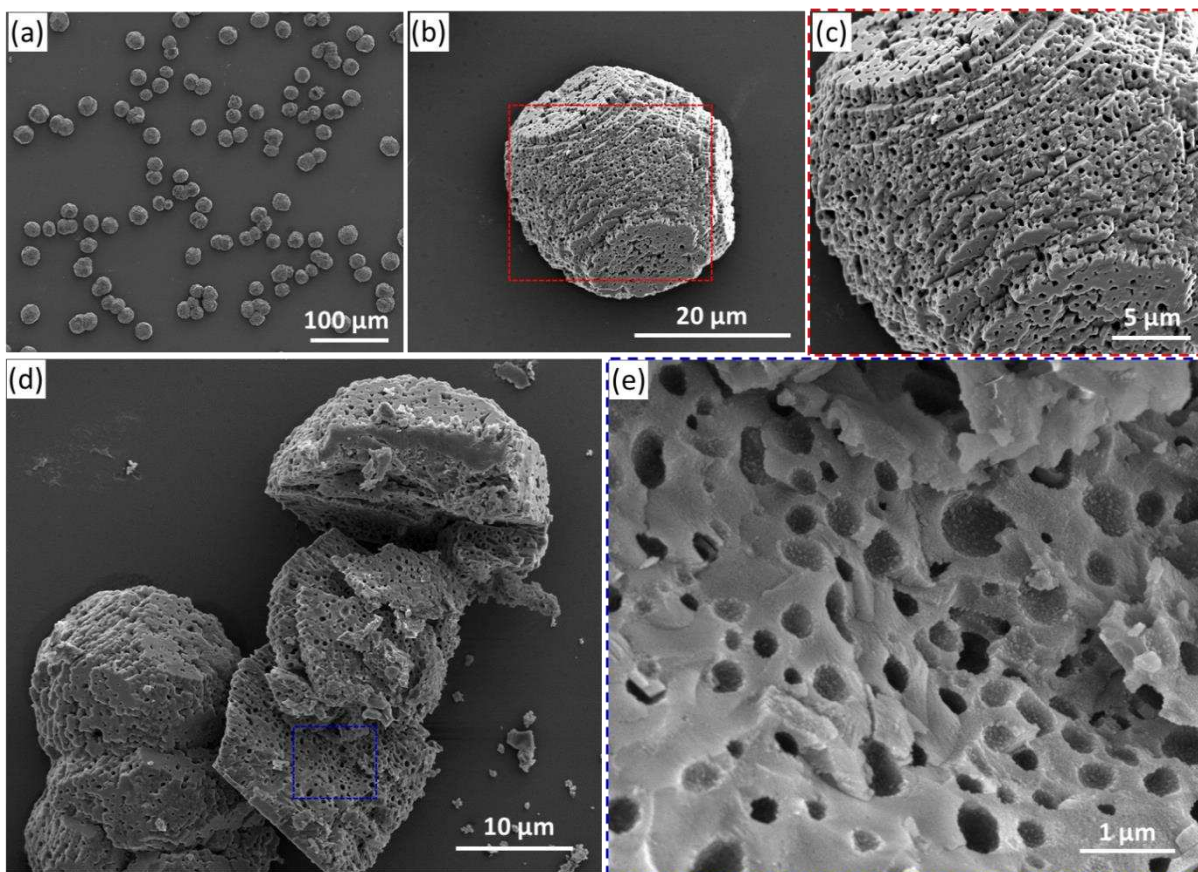


Figure S15. Calcite crystals precipitated in the presence of 7.77 μM silica-loaded G_{54} - H_{350} - E_{25} - MAA_{300} vesicles. (a)~(c) SEM images, where (c) showing a magnified area as indicated in (b); (d) SEM image showing the cross-section of a randomly-fractured crystal; (e) a magnified SEM showing the area as indicated in (d).

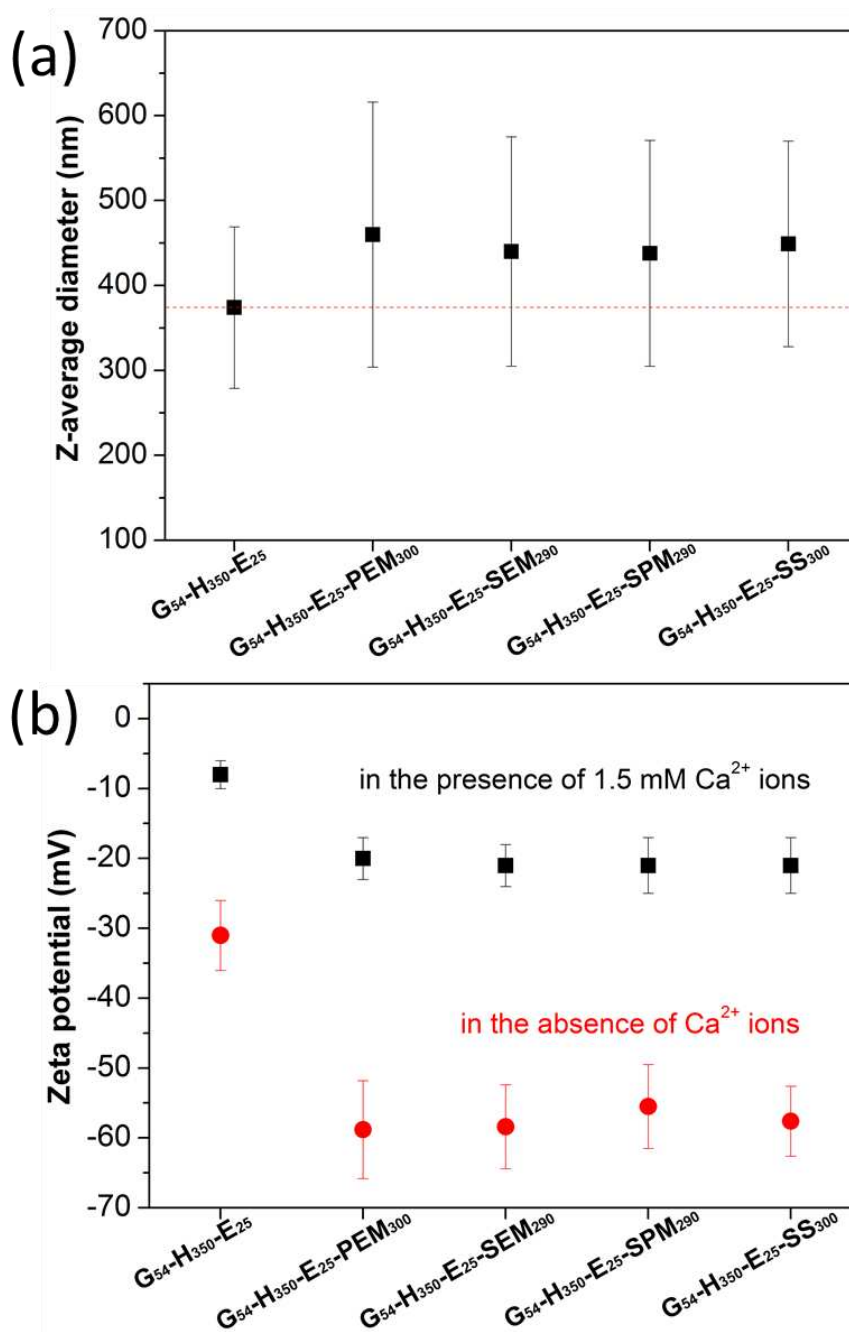


Figure S16. (a) Dynamic light scattering and (b) aqueous electrophoresis data obtained for $\sim 0.1\%$ w/w aqueous dispersions of five types of block copolymer vesicles. According to the former technique, the precursor silica-loaded $G_{54}\text{-H}_{350}\text{-E}_{25}$ vesicles always grew in size after chain extension using 2-(phosphonoxy)ethyl methacrylate, ammonium 2-sulfatoethyl methacrylate, potassium 3-sulfopropyl methacrylate or sodium 4-styrenesulfonate, see **Figure S16a**. **Figure S16b** shows zeta potentials recorded for vesicles in the presence and absence of 1.5 mM Ca^{2+} at pH 9. The significant reduction in negative zeta potential observed in the presence of 1.5 mM Ca^{2+} suggests that these divalent cations bind to the anionic stabilizer chains. N.B. The zeta potential of ~ -30 mV observed for the precursor silica-loaded $G_{54}\text{-H}_{350}\text{-E}_{25}$ vesicles is ascribed to the terminal carboxylic acid groups located at the end of the non-ionic G_{54} stabilizer chains.⁸

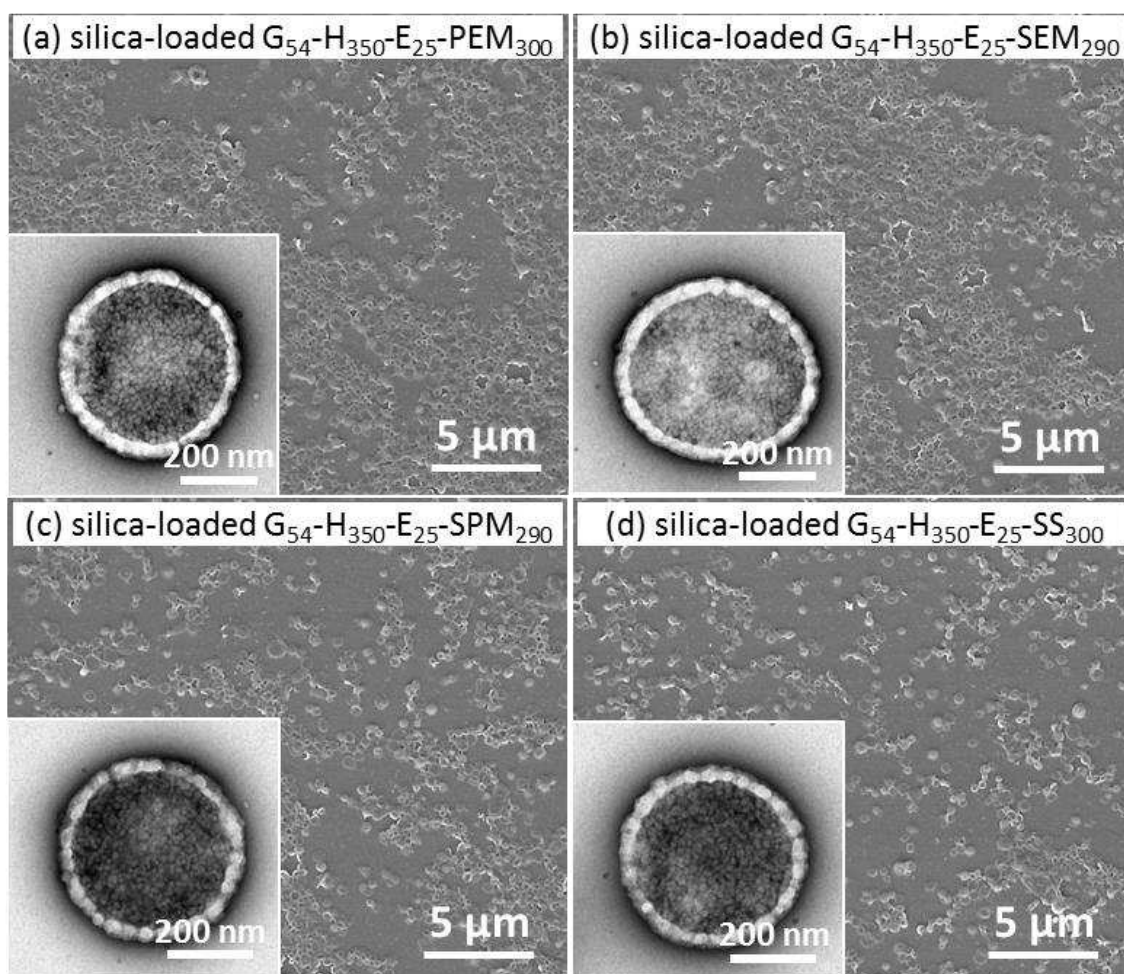


Figure S17. SEM images recorded for silica-loaded covalently cross-linked G_{54} - H_{350} - E_{25} vesicles (containing 17.1% silica by mass) after chain extension with four different anionic monomers: (a) silica-loaded G_{54} - H_{350} - E_{25} - PEM_{300} vesicles; (b) silica-loaded G_{54} - H_{350} - E_{25} - SEM_{290} vesicles; (c) silica-loaded G_{54} - H_{350} - E_{25} - SPM_{290} vesicles and (d) silica-loaded G_{54} - H_{350} - E_{25} - SS_{300} vesicles. Insets show representative high magnification TEM images obtained for individual particles that confirm their vesicular morphology.

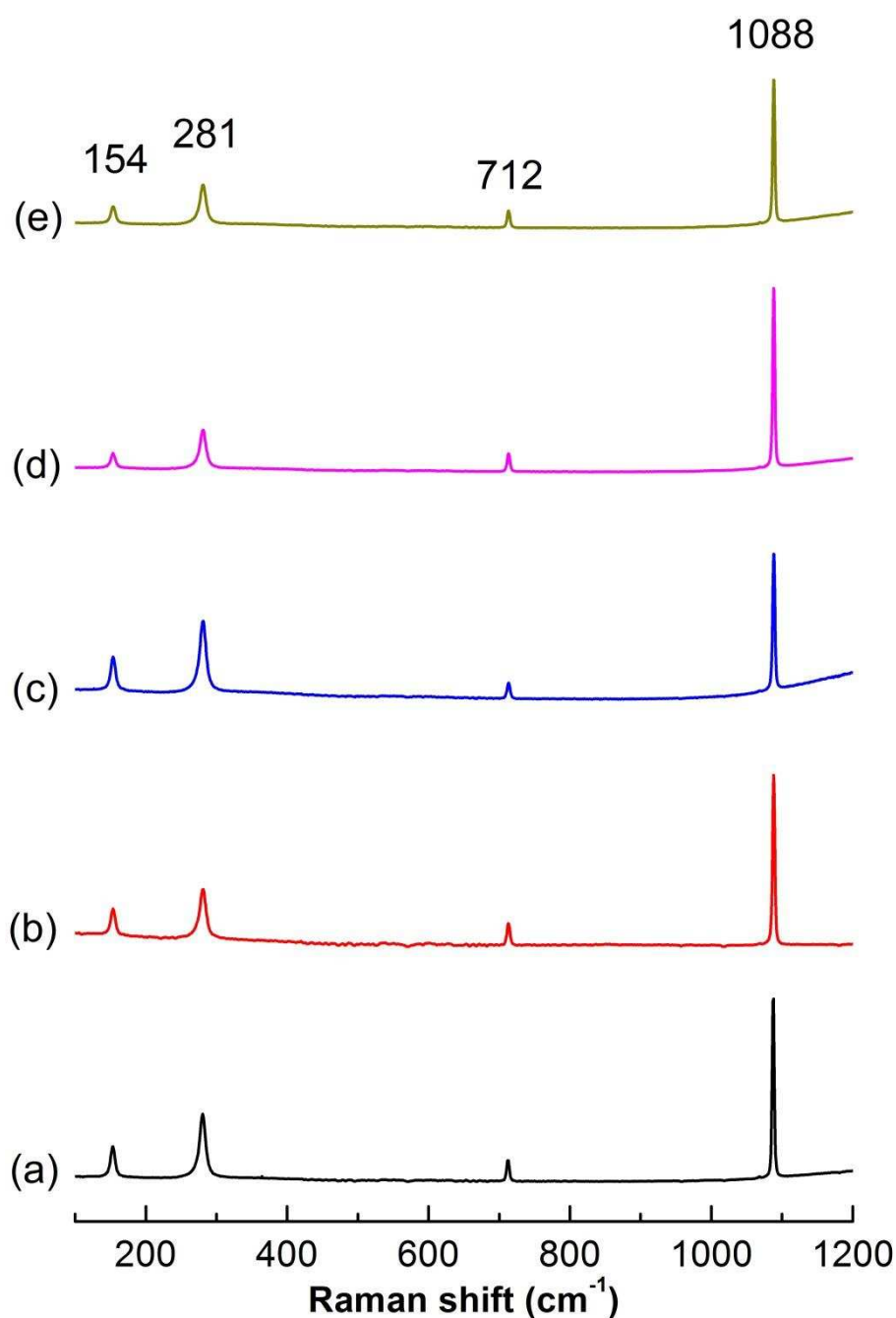


Figure S18. Raman spectra recorded for: (a) a pure calcite control; (b)-(e) calcite crystals precipitated in the presence of a series of silica-loaded vesicles comprising four different anionic stabilizer blocks. More specifically, copolymer compositions for these vesicles (prepared using cross-linked G_{54} - H_{350} - E_{25} precursor vesicles containing 17.1% silica by mass) were: (b) silica-loaded G_{54} - H_{350} - E_{25} - PEM_{300} vesicles, (c) silica-loaded G_{54} - H_{350} - E_{25} - M_{25} - SEM_{290} vesicles, (d) silica-loaded G_{54} - H_{350} - E_{25} - SPM_{290} vesicles, (e) silica-loaded G_{54} - H_{350} - E_{25} - SS_{300} vesicles. Bands appearing at 1088 cm^{-1} (ν_1), 712 cm^{-1} (ν_4), 281 cm^{-1} and 154 cm^{-1} (lattice modes) are characteristic of calcite.⁶⁻⁷

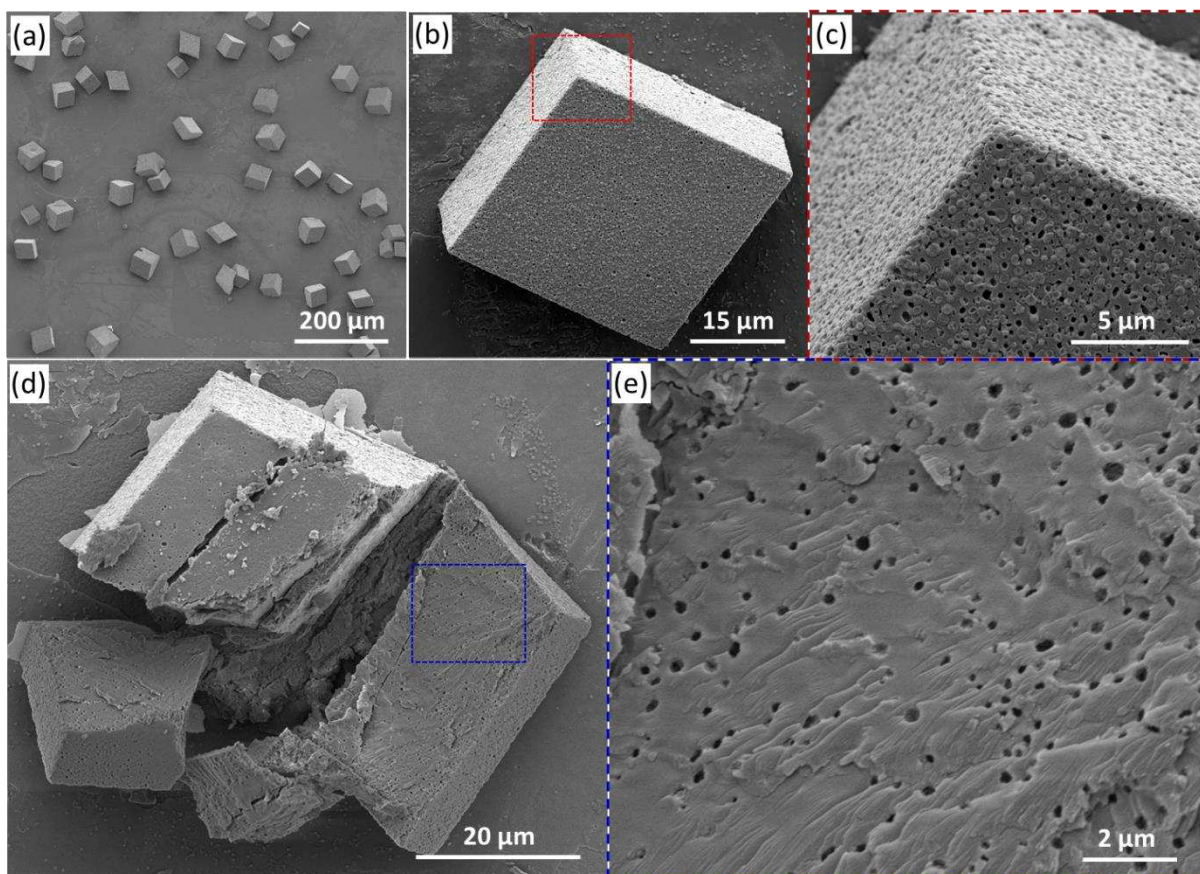


Figure S19. Calcite crystals precipitated in the presence of 7.77 μM silica-loaded G_{54} - H_{350} - E_{25} - PEM_{300} vesicles. (a)~(c) SEM images, where (c) showing a magnified area as indicated in (b); (d) SEM image showing the cross-section of a randomly-fractured crystal; (e) a magnified SEM showing the area as indicated in (d).

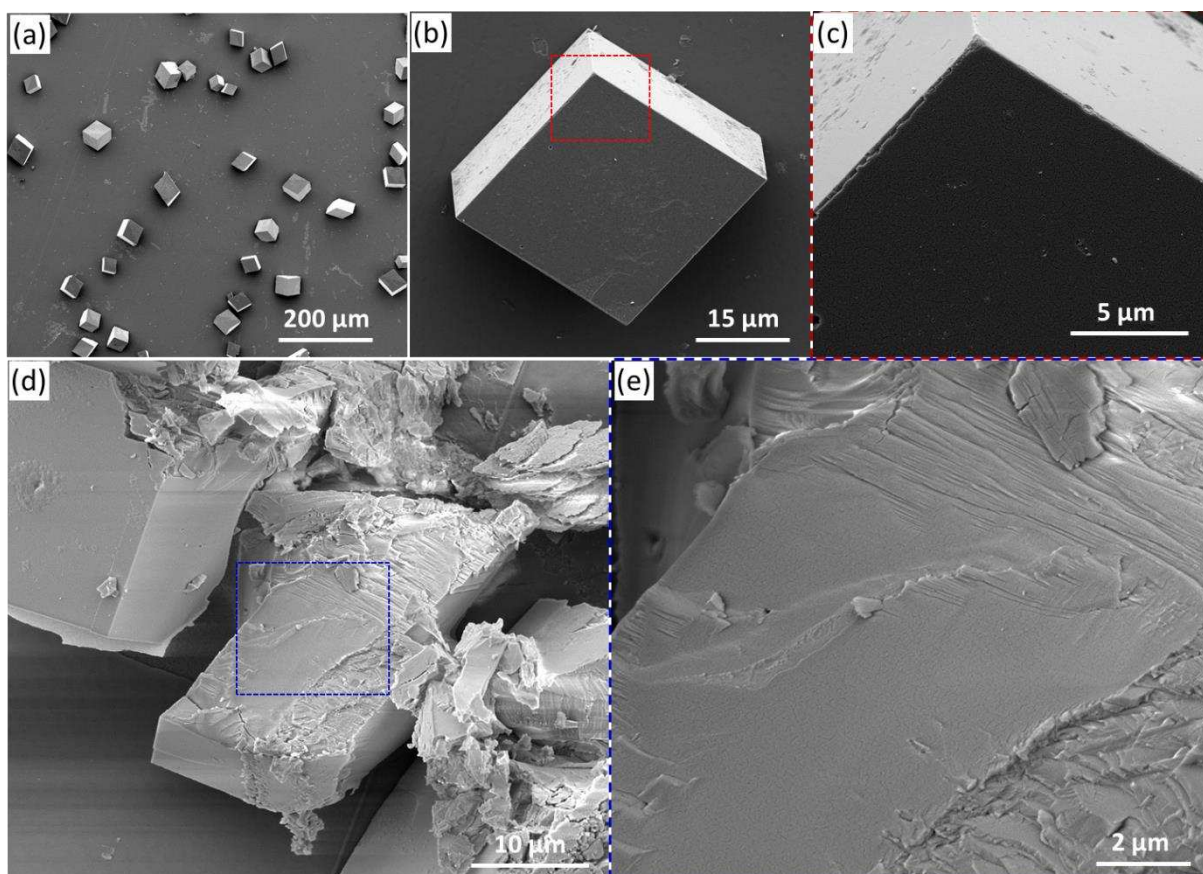


Figure S20. Calcite crystals precipitated in the presence of $7.77 \mu\text{M}$ silica-loaded $\text{G}_{54}\text{-H}_{350}\text{-E}_{25}\text{-SEM}_{290}$ vesicles. (a)~(c) SEM images, where (c) showing a magnified area as indicated in (b); (d) SEM image showing the cross-section of a randomly-fractured crystal; (e) a magnified SEM showing the area as indicated in (d).

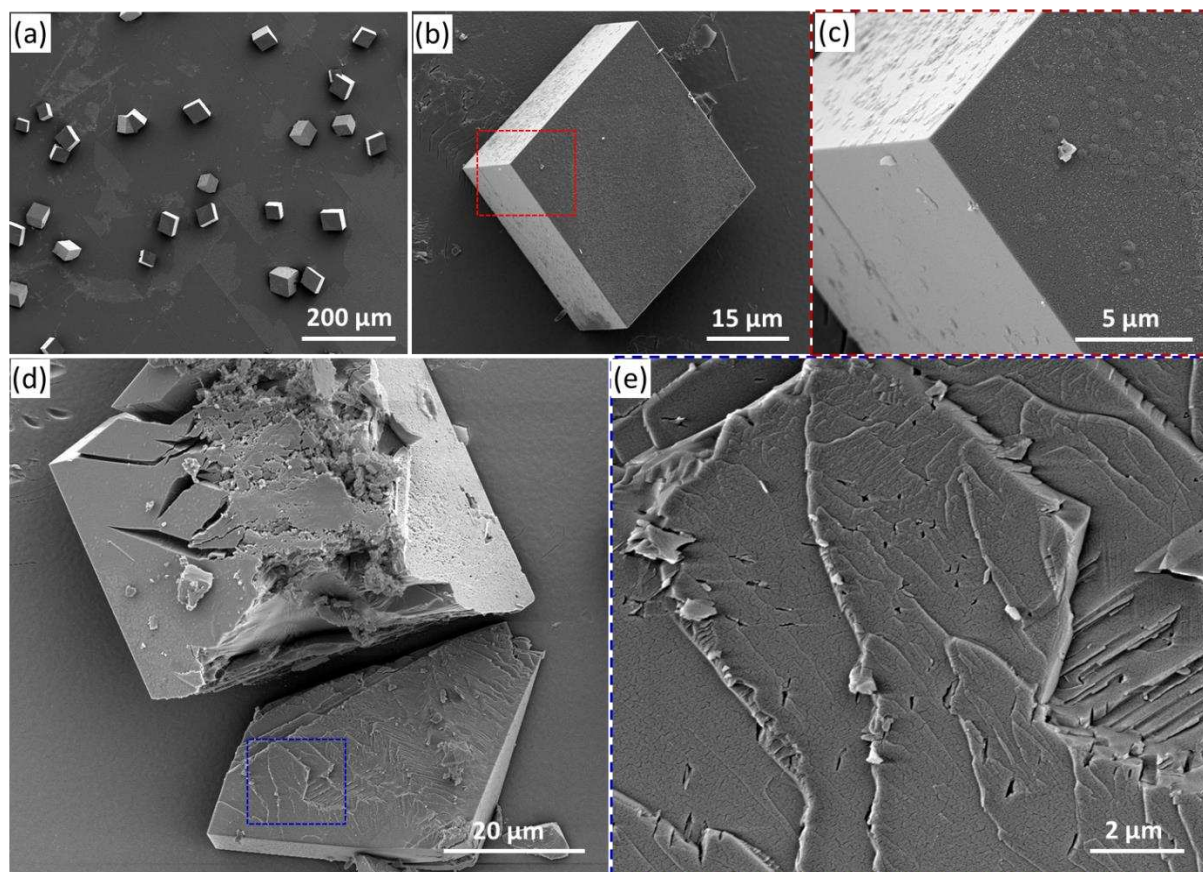


Figure S21. Calcite crystals precipitated in the presence of 7.77 μM silica-loaded G₅₄-H₃₅₀-E₂₅-SPM₂₉₀ vesicles. (a)~(c) SEM images, where (c) showing a magnified area as indicated in (b); (d) SEM image showing the cross-section of a randomly-fractured crystal; (e) a magnified SEM showing the area as indicated in (d).

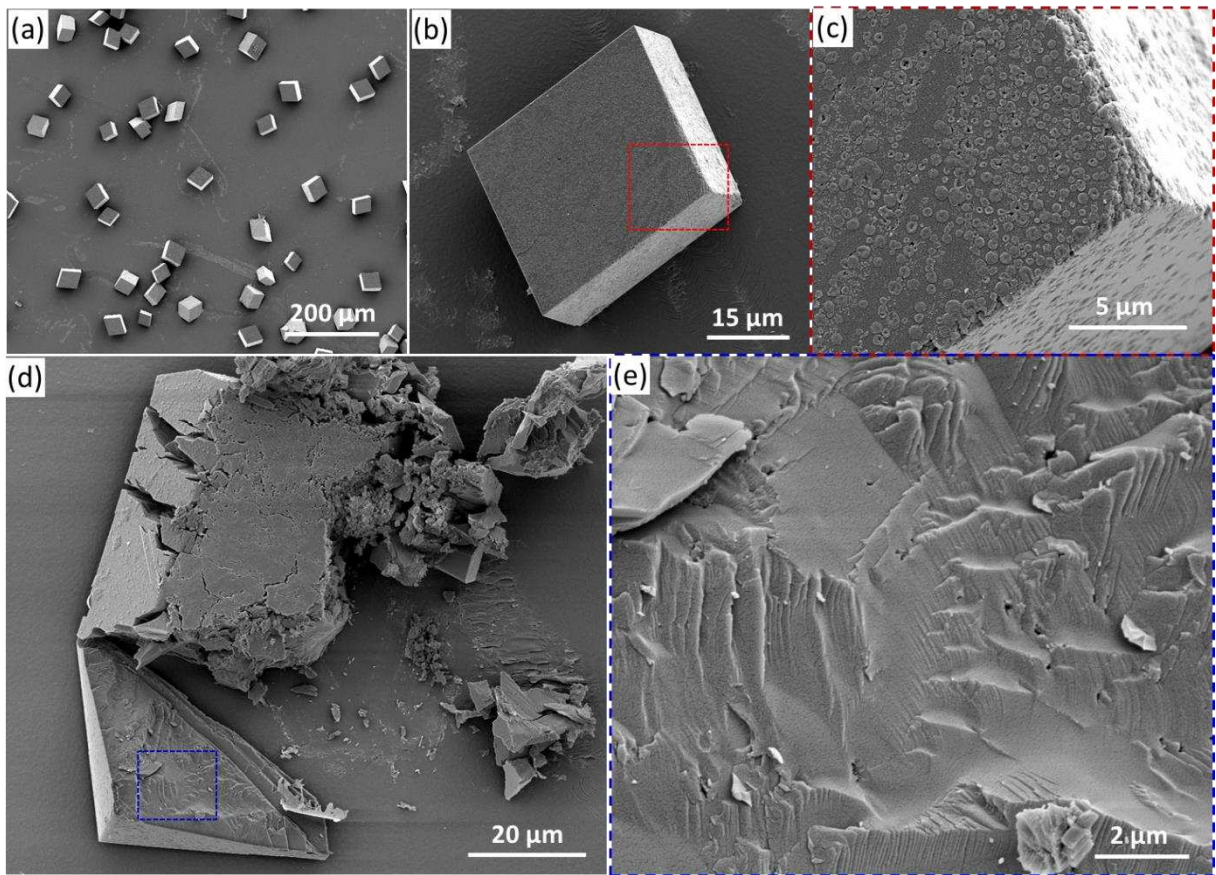


Figure S22. Calcite crystals precipitated in the presence of 7.77 μM silica-loaded $\text{G}_{54}\text{-H}_{350}\text{-E}_{25}\text{-SS}_{300}$ vesicles. (a)~(c) SEM images, where (c) showing a magnified area as indicated in (b); (d) SEM image showing the cross-section of a randomly-fractured crystal; (e) a magnified SEM showing the area as indicated in (d).

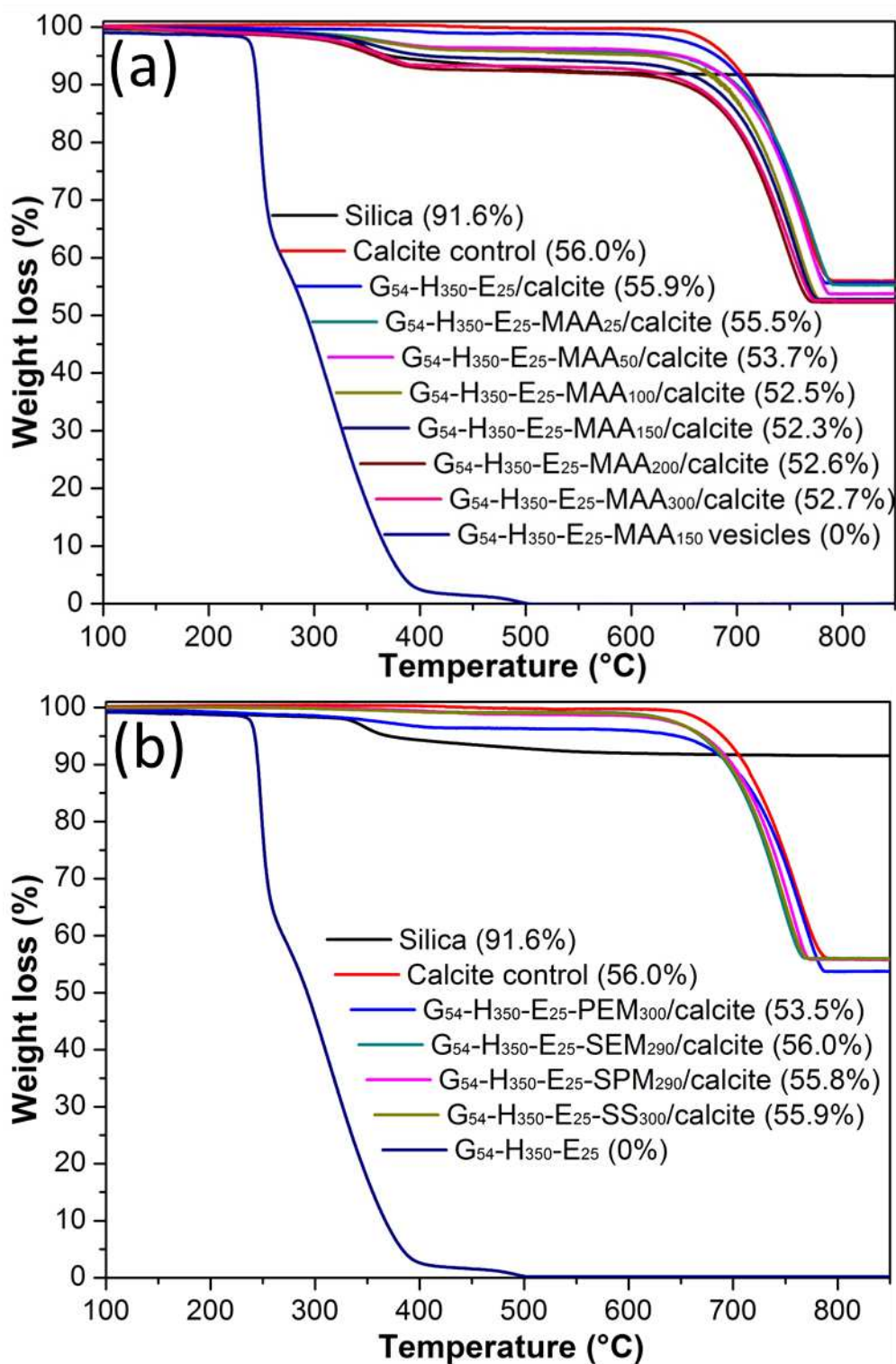


Figure S23. (a) TGA curves recorded for various control samples and calcite crystals precipitated in the presence of silica-loaded G_{54} - H_{350} - E_{25} - MAA_x vesicles where x ranges from 0 to 300; (b) TGA curves recorded for various control samples and calcite crystals precipitated in the presence of vesicles with differing anionic surface functionality.

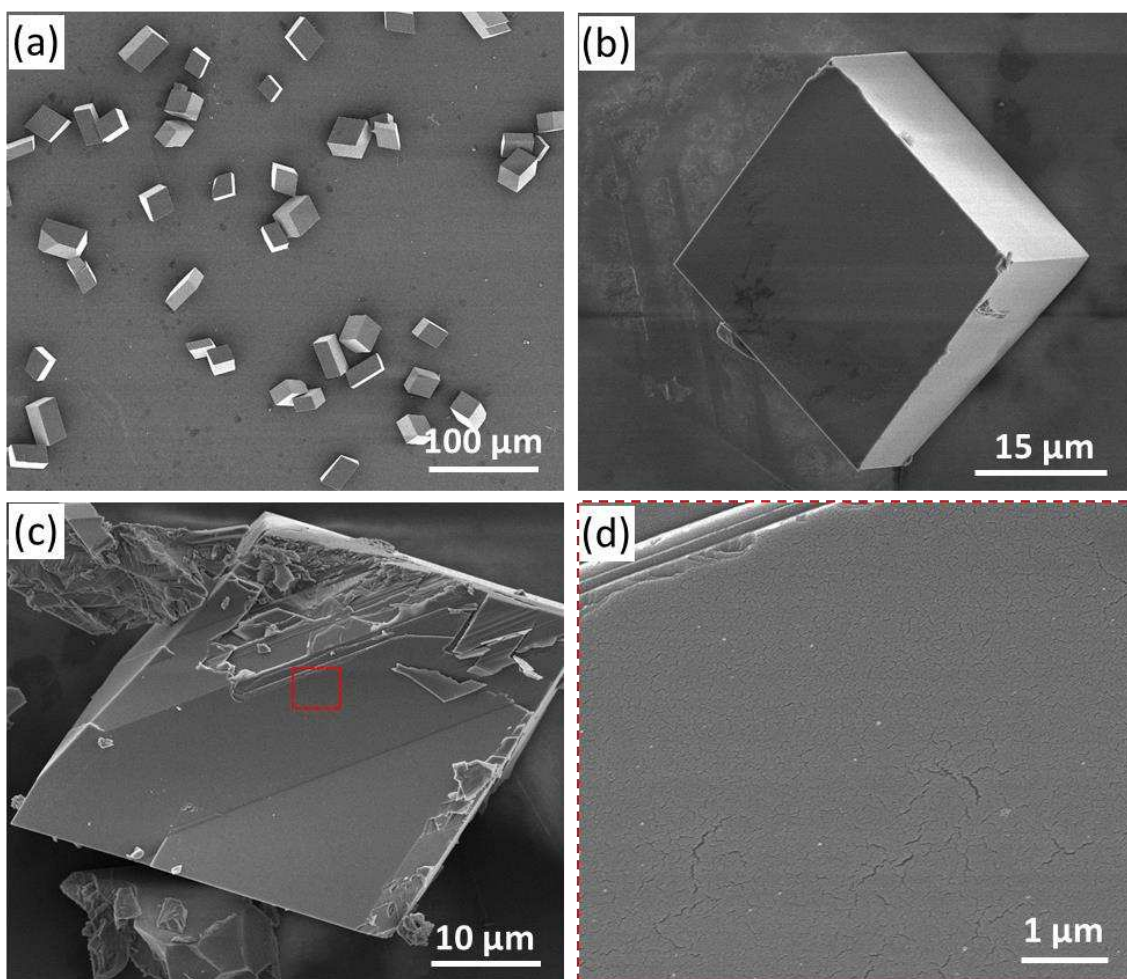


Figure S24. Calcite crystals precipitated in the presence of 0.1 w/w% silica nanoparticles. (a) Low magnification SEM image; (b) SEM images showing an intact calcite crystal; (c) SEM image showing the cross-section of a fractured crystal; (d) a magnified SEM showing the area as indicated in (c).

References

1. Blanazs, A.; Madsen, J.; Battaglia, G.; Ryan, A. J.; Armes, S. P., Mechanistic Insights for Block Copolymer Morphologies: How Do Worms Form Vesicles? *J. Am. Chem. Soc.* **2011**, *133*, 16581-16587.
2. Li, Y.; Armes, S. P., RAFT Synthesis of Sterically Stabilized Methacrylic Nanolatexes and Vesicles by Aqueous Dispersion Polymerization. *Angew. Chem. Int. Ed.* **2010**, *49*, 4042-4046.
3. Chambon, P.; Blanazs, A.; Battaglia, G.; Armes, S. P., Facile Synthesis of Methacrylic ABC Triblock Copolymer Vesicles by RAFT Aqueous Dispersion Polymerization. *Macromolecules* **2012**, *45*, 5081-5090.
4. Deng, R.; Derry, M. J.; Mable, C. J.; Ning, Y.; Armes, S. P., Using Dynamic Covalent Chemistry To Drive Morphological Transitions: Controlled Release of Encapsulated Nanoparticles from Block Copolymer Vesicles. *J. Am. Chem. Soc.* **2017**, *139*, 7616-7623.
5. Mable, C. J.; Gibson, R. R.; Prévost, S.; McKenzie, B. E.; Mykhaylyk, O. O.; Armes, S. P., Loading of silica nanoparticles in block copolymer vesicles during polymerization-induced self-assembly: encapsulation efficiency and thermally-triggered release. *J. Am. Chem. Soc.* **2015**, *137*, 16098-16108.
6. Gabrielli, C.; Jaouhari, R.; Joiret, S.; Maurin, G., In situ Raman spectroscopy applied to electrochemical scaling. Determination of the structure of vaterite. *J. Raman Spectrosc.* **2000**, *31*, 497-501.
7. Wehrmeister, U.; Soldati, A. L.; Jacob, D. E.; Haeger, T.; Hofmeister, W., Raman spectroscopy of synthetic, geological and biological vaterite: a Raman spectroscopic study. *J. Raman Spectrosc.* **2010**, *41*, 193-201.
8. Lovett, J. R.; Warren, N. J.; Ratcliffe, L. P.; Kocik, M. K.; Armes, S. P., pH-Responsive Non-Ionic Diblock Copolymers: Ionization of Carboxylic Acid End-Groups Induces an Order-Order Morphological Transition. *Angew. Chem. Int. Ed.* **2015**, *54*, 1279-1283.